AD NUMBER

AD902566

LIMITATION CHANGES

TO:

Approved for public release; distribution is unlimited.

FROM:

Distribution authorized to U.S. Gov't. agencies only; Test and Evaluation; APR 1972. Other requests shall be referred to Army Air Mobility Research and Development Lab., Fort Eustis, VA.

AUTHORITY

USAAMRDL ltr 30 Mar 1970

AD

USAAMRDL TECHNICAL REPORT 72-15

DESIGN, FABRICATION, AND PERFORMANCE TESTING OF INTEGRAL ARMORED SERVO ACTUATORS

FINAL REPORT

By

K. Wallischeck
G. Karas

April 1972

EUSTIS DIRECTORATE
U. S. ARMY AIR MOBILITY RESEARCH AND DEVELOPMENT LABORATORY
FORT EUSTIS, VIRGINIA

CONTRACT DAAJ02-70-C-0051 New
UNITED AIRCRAFT CORPORATION
SIKORSKY AIRCRAFT
STRATFORD, CONNECTICUT

DISCLAIMERS

The findings in this report are not to be construed as an official Department of the Army position unless so designated by other authorized documents.

When Government drawings, specifications, or other data are used for any purpose other than in connection with a definitely related Government procurement operation, the U. S. Government thereby incurs no responsibility nor any obligation whatsoever; and the fact that the Government may have formulated, furnished, or in any way supplied the said drawings, specifications, or other data is not to be regarded by implication or otherwise as in any manner licensing the holder or any other person or corporation, or conveying any rights or permission, to manufacture, use, or sell any patented invention that may in any way be related thereto.

Trade names cited in this report do not constitute an official endorsement or approval of the use of such commercial hardware or software.

DISPOSITION INSTRUCTIONS

Destroy this report when no longer needed. Do not return it to the originator.

DEPARTMENT OF THE ARMY
U. S. ARMY AIR MOBILITY RESEARCH & DEVELOPMENT LABORATORY
EUSTIS DIRECTORATE
FORT EUSTIS, VIRGINIA 23604

This report was prepared by Sikorsky Aircraft Division, United Aircraft Corporation, under the terms of Contract DAAJ02-70-C-0051. NEW

In an effort to improve the ballistic protection for complex Army aircraft critical components, the objective of this program was to design and fabricate dual property steel armor (DPSA) as an integral part of a critical aircraft component (in this case, a servo actuator), while maintaining functional and operational response characteristics similar to those of the standard component. The advanced technology was successfully demonstrated by using DPSA integrally in a redesigned experimental CH-54B primary flight control hydraulic servo actuator through fabrication and testing of three units, reducing vulnerable areas, eliminating or minimizing the amount of armor plate shielding required and retaining easier access to the servo for maintenance purposes.

Technical direction and monitorship of this contract were provided by Mr. Earl Gilbert and Mr. Stephen Pociluyko of the Safety and Survivability Division.

DA
Project 1F164204D154
Contract DAAJ02-70-C-0051
USAAMRDL Technical Report 72-15
April 1972

DESIGN, FABRICATION, AND PERFORMANCE TESTING OF INTEGRAL ARMORED SERVO ACTUATORS

Final Report

By
K. Wallischeck
G. Karas

SER-50759

Prepared by

United Aircraft Corporation
Sikorsky Aircraft
Stratford, Connecticut

for

EUSTIS DIRECTORATE
U.S. ARMY AIR MOBILITY RESEARCH AND DEVELOPMENT LABORATORY
FORT EUSTIS, VIRGINIA

323 800

SUMMARY

The program summarized by this report was conducted to demonstrate and establish the applicability of using Dual Property Steel Armor (DPSA) integrally in complex Army aircraft critical components, thus eliminating or minimizing the requirement for adding armor plate (shielding) to protect these components from small-arms ballistic impacts. A CH-54B primary flight control hydraulic servo actuator was selected as the critical component and has been redesigned using DPSA as the cylinder material with three experimental units fabricated and tested under this contract.

The functional and response characteristics of the integral DPSA servo actuator are equivalent to those of the primary servo now operational on the CH-54B helicopter. The components have been analyzed for structural adequacy using criteria established for the CH-54B. Also, the servo has been analyzed for function and stability. These analyses show that the integral armored servo is structurally adequate and that the function and performance will be satisfactory.

The servo and mounting bracketry and manifold shield are considerably heavier than the servo and armor plate now used on the CH-54B. However, greater than 75% protection of the exposed vulnerable areas of the conventional servo with armor is provided with the advantages of elimination of large armor plate surfaces for protection and the difficulty of access to maintain the servo by removal of this heavy excess armor plate. A weight reduction effort can reduce the weight to be more competitive.

FOREWORD

This report covers the design, fabrication and test of a primary flight control hydraulic servo mechanism using dual property steel armor as a structural material. The program was conducted for the Eustis Directorate under Contract DAAJ02-70-C-0051, Project 1F164204D154.

Eustis Directorate technical direction was provided by Mr. S. Pociluyko and Mr. E. Gilbert.

The principal contributors for Sikorsky Aircraft were Messrs. G. R. Karas, Task Manager; D. Wilson, Mechanical Systems Test Group; G. Kudasch, designer; K. Wallischeck, designer; K. Farkas, Supervisor Hydraulics Laboratory; and P. Targonski, Senior Technician.

TABLE OF CONTENTS

LIST OF ILLUSTRATIONS

LIST OF TABLES

LIST OF SYMBOLS

A	area, sq in.
A_p	piston area, sq in.
A_s	shear area, sq in.
A_t	tensile area, sq in.
a	feedback ratio
B	bulk modulus, psi
C_A	aerodynamic damping, lb-sec/in.
C_D	leakage coefficient, $in.^5$/lb-sec
C_d	orifice coefficient
C_p	pressure coefficient, $in.^5$/lb-sec
C_v	flow coefficient, $in.^2$/sec
C_s	swash-plate damping, lb-sec/in.
C_1	valve coefficient
C_2	valve coefficient
C_3	fuselage structural damping, lb-sec/in.
c	distance from cg to fiber of interest, in.
cg	center of gravity
D,d	diameter, in.
d_b	bending deflection, in.
d_s	shear deflection, in.
D_o	outer diameter, in.
D_i	inner diameter, in.
E	modulus of elastricity, psi
F	force, lb
f_r	reliability factor

f_s	size effect factor
f_{su}	surface effect factor
f_t	stress reduction factor
F_n	normal force, lb
F_v	force, vibratory, lb
F_s	force, steady, lb
G	shear modulus, psi
g	gravitational acceleration, $in./sec^2$
gpm	gallons per minute
hp	horsepower
Hz	cycles per second
I	moment of inertia, $in.^4$
K	spring constant, general, lb/in.
K_a	aerodynamic spring, lb/in.
K_f	cycle dependent fatigue stress concentration factor
K_p	pressure gain, psi/in.
K_t	fatigue stress concentration factor
K_V	flow gain, $in.^2/sec$
K_1	combined swash plate and torsional blade stiffness, lb/in.
K_2	equivalent fuselage stiffness, lb/in.
K_5	support spring stiffness, lb/in.
k	hydraulic conductance, $in.^3/sec-lb$
L	length, in.
m	slope
M_1	equivalent blade mass, $lb-sec^2/in.$

M_2	equivalent pylon mass, lb-sec^2/in.
M_3	equivalent fuselage mass, lb-sec^2/in.
M	moment, in.-lb
MS	margin of safety
N	number of cycles
P	pressure, psi
Q	flow, in.^{3}/sec
R	vibratory load ratio, minimum to maximum
R_A	vertical reaction force, lb
R_B	horizontal reaction force, lb
S	stress, psi
S_{aa}	stress allowable amplitude for lugs, psi
S_{as}	stress allowable amplitude for a specific lug, psi
S_b	stress, bearing, psi
S_s	stress allowable, static, shear, ultimate, psi
S_{tu}	stress allowable, static, tension, ultimate, psi
S_{ty}	stress allowable, static, tension, yield, psi
S_{en}	stress allowable, fatigue, tension, psi
S_{cn}	stress allowable, fatigue, compression, psi
S_{cy}	stress allowable, static, compression, yield, psi
S_s	stress, shear, psi
S_{su}	maximum shear stress, psi
S_t	stress, tension, psi
S_M	stress, steady, mean, psi
S_V	stress, variable, $\pm$ psi
T	torque, in.-lb

t	time constant, sec
u	Poisson's ratio
V	volume, $in.^3$
V_r	volumetric ratio
$\dot{W}$	density, $lb/in.^3$
W_B	break frequency, rad/sec
X	displacement, in.
X_p	piston displacement, in.
X_v	valve displacement, in.
ε	strain, in.
θ,ϕ	angles, deg
μ	coefficient of friction
ν	viscosity, centipoise
π	ratio of circumference to diameter
σ	maximum shear stress, psi

BACKGROUND

The flight control system in helicopters enables the pilot to control the pitch of the rotor blades and thus the resultant thrust vector of the rotor system. Although the details of design of the systems vary between manufacturers, most systems are mechanical and employ some type of power boost to aid the pilot in maintaining blade pitch control. On the larger helicopters, the aerodynamic induced loads can be so high that power operation is mandatory for safe flight. In this event, usually redundant hydraulic cylinder-operated power systems, called servo actuators, are supplied, and when the aircraft is to operate in a hostile environment, armor protection is often provided to critical elements of the system. The flight control primary servos are considered to be critical elements of the control systems of large modern helicopters. Figure 1 represents the location of the primary flight control servos in the CH-54 helicopter. Figure 2 shows details of the primary servos mounted on a main rotor transmission along with the armor plate protection. Where shielding is provided by adjacent structure, no armor is provided. Typically, the armor shown in Figure 2 shields only those components which offer the greatest projected area. In this installation, this is basically the primary servo housing. The servo valves mounted on the housing are also protected.

This program was conducted to demonstrate and establish the applicability of fabricating a primary flight control servo actuator using dual property steel armor (DPSA) as an integral structural material, thus eliminating the need for or minimizing armor protection and decreasing the vulnerability to caliber .30 AP M2 projectile impacts. This servo was to be compatible with the CH-54B helicopter functional requirements and installation constraints. Because of the specific properties of the DPSA barrel, some modification to the basic servos used on the CH-54B aircraft was necessary. Balanced stages for the tandem servos have been incorporated, and the hydraulic communication porting within the servo is inside the power piston for increased protection. DPSA material in the plate form has been utilized to provide protection to other critical areas of the primary servo which were not protected by the integration of DPSA material.

The current primary flight control servo used on the CH-54B helicopter is a two-stage positional servo powered by two separate hydraulic systems. The stages are located in tandem and share a common power piston, feedback link and trunnion for mounting onto the main rotor transmission housing. Each stage is provided with a servo valve which controls the direction and rate of fluid application to the cylinders. When the valve spool is displaced to either side of null, fluid under pressure is directed to one side of the piston head and the other side is vented to return pressure. This pressure differential acting upon the effective piston area results in a force which drives the piston. When the input to the valve is held in a fixed position, the feedback link, which is attached to the output side of the piston, causes the servo valve to assume the center or null position, and the servo will maintain its position. A cutaway view showing the details of the servo is presented in Figure 3.

Figure 1. CH-54B Helicopter.

Figure 2. Primary Flight Control
Servo and Armor Installation.

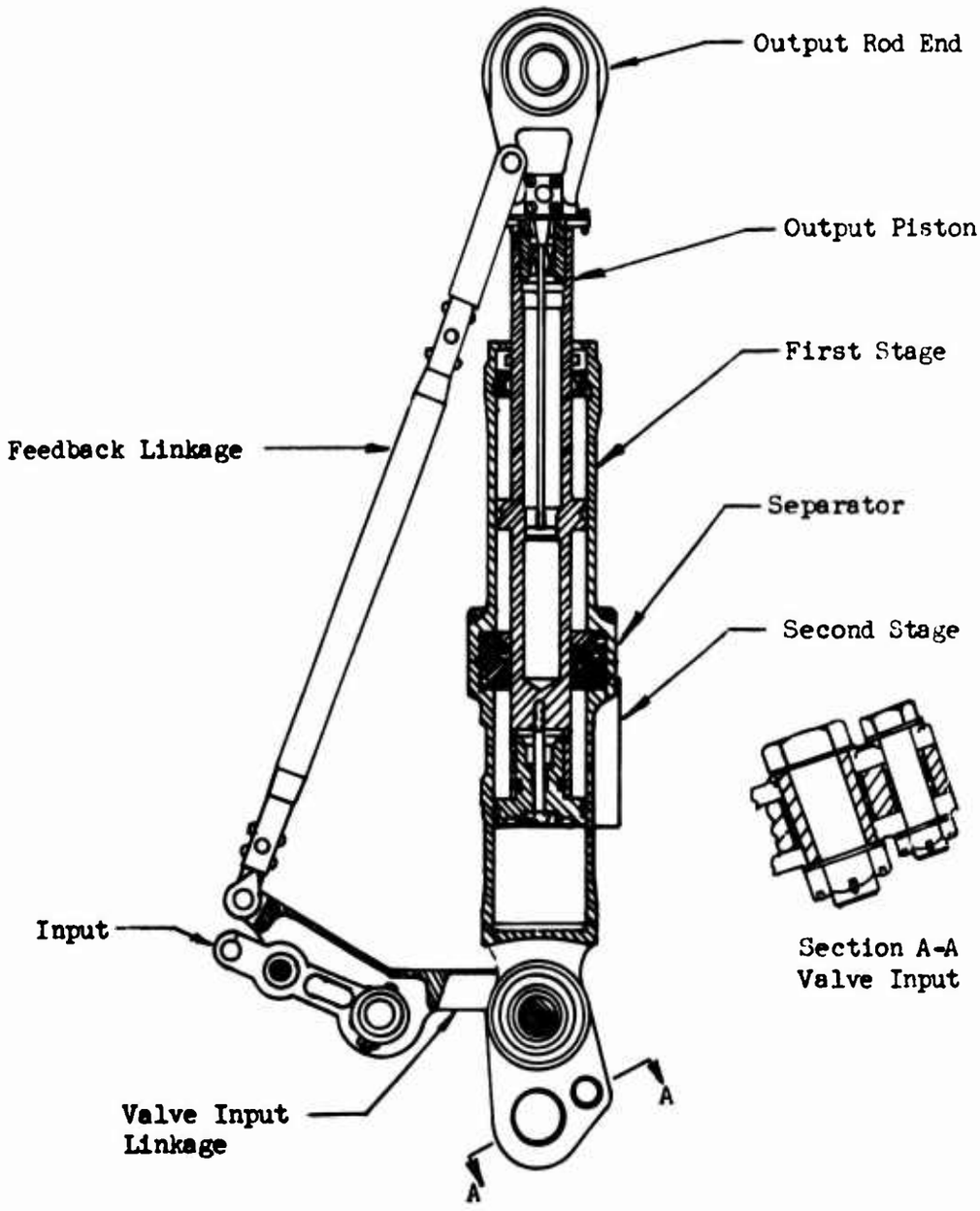

Figure 3. Cutaway View,
Standard Configuration.

On the aircraft, the primary servos are protected from small-arms damage by armor plate. See Figure 2 for details. The areas shielded include the housing and servo valves. The input links, feedback link and output piston are not protected. The armor protection shields most of the critical areas of the servo. However, damage to the unprotected elements can result in the loss of servo power operation or, in some cases, can cause the servo to drive to a hard-over position. For example, a projectile impacting on the power piston may not cause a structural failure, but can cause a surface imperfection which would impede piston travel through the housing. Since the clearance between the piston and housing end cap is small (0.005 in.), only a small surface imperfection would result in a jammed servo. A separation in the feedback link would interrupt the valve recentering function, and the servo could drive to a hard-over position. Either of these conditions could result in uncontrolled flight. Although the projected areas of these elements are relatively small, the amount of additional armor needed for shielding is high. Thus, cost effectiveness dictates that these elements not be protected by armor. However, damage to these critical components can cause uncontrolled flight.

INTEGRAL ARMORED SERVO

DESIGN

The integral armored servo utilizes DPSA as an integral structural material. Both housings of the tandem servo and the servo valve manifold shield are made from DPSA. The wall thickness of the housing is such that a caliber .30 AP M2 projectile with a velocity of 2750 feet per second will not penetrate or dent the housing sufficiently to cause servo binding. A hood of DPSA is welded onto the end of the first-stage cylinder to protect the piston from being dented when the piston is extended; this could prevent subsequent retraction. Also, the servo is of a concentric design and the feedback path is through the piston itself, which is fully protected. See Figure 4 for cutaway details. The hydraulic manifolds are separate and installed so that they are shielded by the transmission housing on one side and the servo housing on the other. Thus, the servo not only incorporates those features necessary to provide the same degree of protection as the current design, but also provides protection in other critical areas. Figure 5 is a photograph of the integral armored servo components. Figure 6 is a photograph of the assembly.

The integral armored servo incorporates state-of-the-art features which have been developed by Sikorsky Aircraft for improved safety and reliability for flight control actuators. The housing is fabricated from two separate sections rather than from one piece with internal separators. Because of the two-piece housing construction, a crack developing in one housing cannot propagate into the other. Thus, separation between the redundant stages is enhanced.

Integral filters protect the lapped servo valves from contaminants and thereby reduce the probability of valve jamming. A jammed valve could cause a hard-over type malfunction. To further improve the valve reliability, a unique two-piece spool and failure detection means are used. In normal operation, only a few pounds are required to displace the spool within its sleeve. See Figure 7 of the hydraulic schematic for details.

A jammed valve can require many hundreds of pounds for operation and, in extreme conditions, may fail before the block can be overcome. The two-piece spool incorporates a concentric inner spool which is normally fixed with respect to the main spool by preloaded springs. If the main spool should jam, the inner spool will move and place the servo into a bypass or inactive condition. Motion of the inner spool also opens a port which causes a pressure switch to signal a jammed valve condition to the pilot.

WEIGHT VERSUS REDUCTION OF VULNERABLE AREA

The integral armored servo assembly weighs 79 lb, the support bracket weighs 11 lb, and the valve manifold armor weighs 29 lb. Thus, the total weight of the servo installation which can be used on the CH-54B helicopter is 119 lb. The weight of the existing primary servo and its armor for caliber .30 AP M2 is 75.4 lb. The weight delta is then 43.6 lb per servo. It is estimated that this can be reduced to less than 20 lb

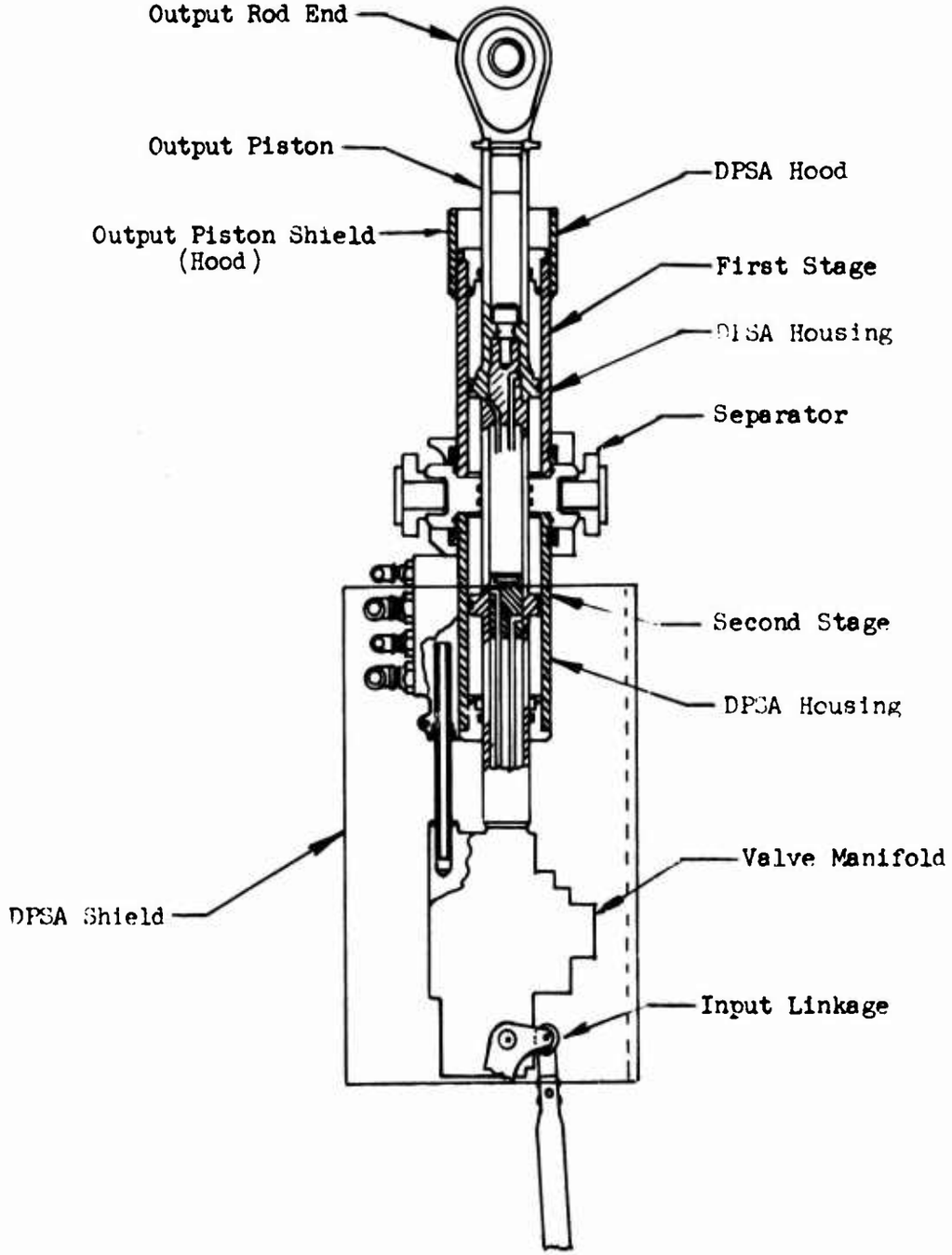

Figure 4. Cutaway View,
Integral Armored Servo.

Figure 5. Integral Armored Servo Components.

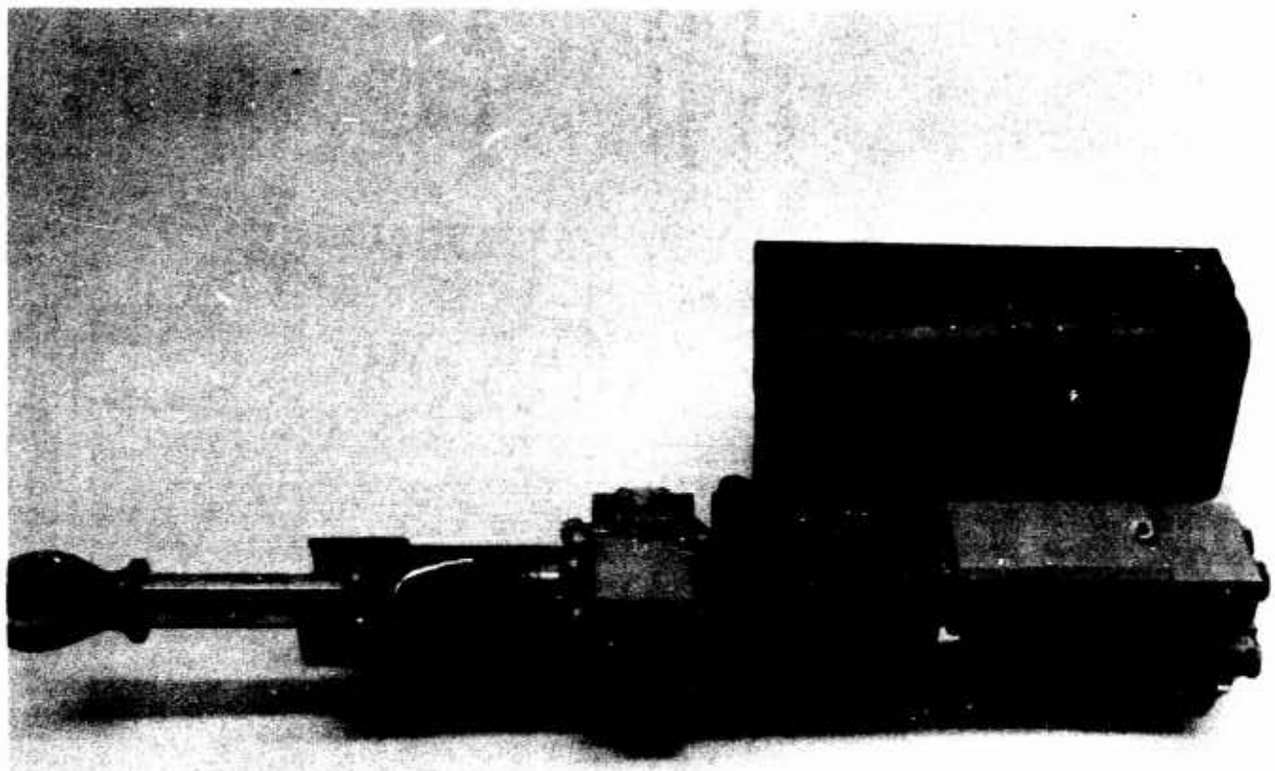

Figure 6. Integral Armored Servo Cylinder Assembly.

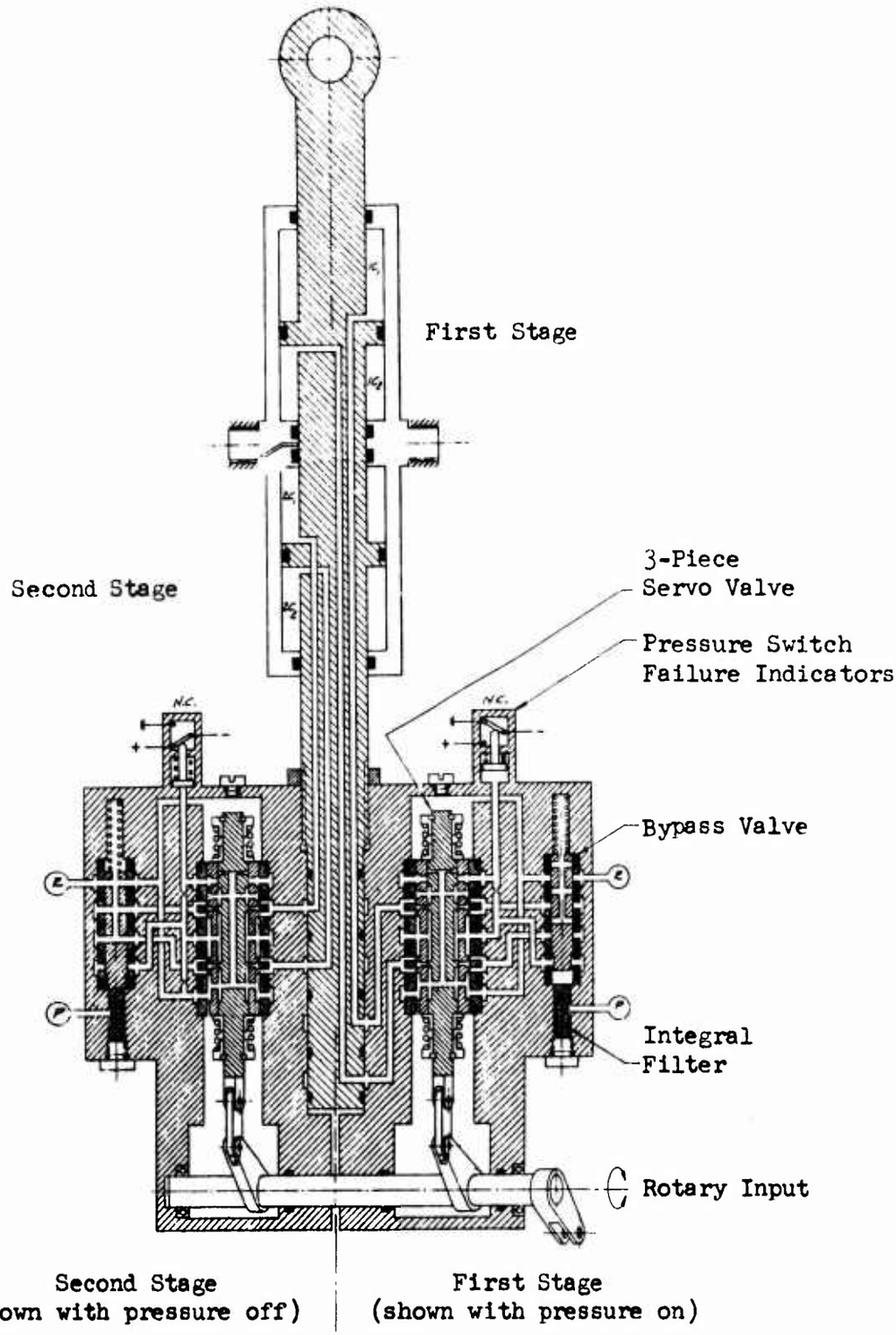

Figure 7. Integral Armored Servo Hydraulic Schematic.

per servo by refinement of the design and reducing the size of the manifold shield.

This weight differential results from several factors:

1. Parts are machined from solid stock. The use of forgings could reduce the weight of the servo assembly for a production version. The scope of this program did not warrant the cost of forgings.

2. The servo mounting points were dictated by the geometry of the existing aircraft. This led to a large support bracket (11 lb).

3. The valve manifold shield is large (29 lb). The use of DPSA material to fabricate the manifold and thus eliminate the armor can be considered for future designs. The available cylindrical extrusions are too small for this appliction. As an alternative, a reduced level of protection can be considered with a corresponding reduction in shielding weight.

4. The cylinder barrels are much heavier than conventional materials would be since wall thickness is determined by ballistic tolerance requirements, and not stresses. In new designs, higher system pressures could be employed to reduce the size of the components while retaining the same wall thickness for ballistic tolerance.

Although the weight delta in comparison to the existing primary servo and its armor is greater than desired, the reduction in vulnerable area is calculated to be 75%, thus improving the state of the art of helicopter survivability. See Figure 8 for a comparison of the standard armor-shielded servo versus the DPSA design.

STRESS ANALYSIS

The components used in the integral armored servo have been analyzed for structural integrity based upon the most stringent loads applied to the components. Both static and vibratory loads have been considered. The analysis is shown in detail in Appendix I.

Static loads are basically those which result from system hydraulic pressure. The system is rated at 3000 psi operating, 4500 psi proof and 7500 psi burst pressure.

Dynamic or vibratory loads result from the aerodynamic forces imposed upon the rotor system transposed to the output rod end on the servos. These forces are traced through the servo by static analysis and are eventually reacted by the mounting bracket which attaches to the main rotor transmission. The installation points of the integral armored servo are the same as those of the existing servo on the CH-54B. The vibratory loads used in the analysis are based upon loads measured on the CH-54B model aircraft during flight testing and are conservative. Consideration has been given to size, notch sensitivity, surface conditions and material

Integral Armored Servo

Standard Servo
With Armor Plate

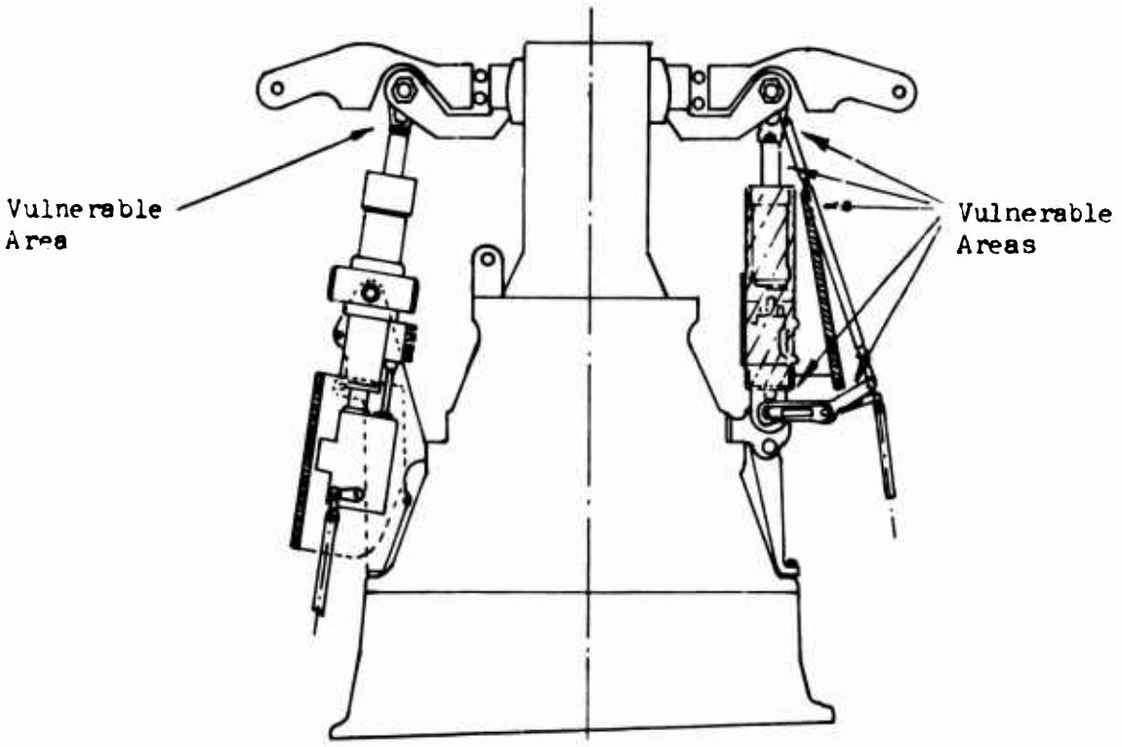

Vulnerable Areas	
Integral Armored Servo	**Standard**
Output Rod End	Output Rod End
	Output Piston
	Feedback Linkage
	Input Linkage
	Valve Input

Figure 8. Vulnerable Area of Standard Servo and Integral Armored Servo.

variability effects. The values used for these various factors are based upon experience accumulated at Sikorsky Aircraft and are conservative. The techniques employed are standard at Sikorsky Aircraft, and are in accord with general aircraft design practice.

The material properties used are in accord with general practice used at Sikorsky Aircraft with one exception. There is no published data on the fatigue properties of DPSA. For the analysis, it has been assumed that the properties are similar to those of conventional alloy steel.

The criteria applied to all components are as follows:

Static

No damage or detrimental deformation of any component up to proof pressure conditions. Ultimate stress will not be exceeded at burst pressure conditions.

Dynamic

Components subjected to dynamic loads will not require replacement at less than 10,000 aircraft hours based upon normal loading spectrum encountered in flight.

Functional

Where elastic deformation would interfere with proper operation of the servo, components shall be designed to provide the proper stiffness even though the structural properties would greatly exceed the static and dynamic requirements.

The analysis summarized in Appendix I demonstrates that the components satisfy all of the criteria listed above.

STABILITY ANALYSIS

Stability is essential in a primary flight control system. Further, it is not sufficient for any portion of the system to be stable by itself, but each component must be stable when operating under the influence of the complete system. The flight control system of a helicopter is a dynamic system containing the fuselage and rotor head characteristics, and as such is best expressed in matrix form. This matrix can then be solved with the aid of the computer. There are several different methods available to perform a stability analysis on a system: the Bode, Nyquist, Nichols or Roothous method. For this analysis the Roothous approach was followed because of the complexity involved and the availability of computer programs capable of solving the problem for the characteristic equation of the total system. From the roots of the characteristic equation, stability can be predicted. For the armored servo, it was found that the real part of all roots was negative, which upon transformation results in a solution having only decaying exponentials. For details of the stability analyses, see Appendix II.

TEST PROGRAM

Three servos were fabricated, assembled and tested in accordance with standard acceptance test requirements for CH-54B primary servos. One unit was subjected to additional tests designed to demonstrate the characteristics of the servo to be comparable to the standard servo. These additional tests included flow gain and pressure gain characteristics of the servo valve, the spring rate of the input linkage and the frequency response characteristics of the servo assembly. The detailed test plan, test notes and characteristic curves are included in Appendix III.

The test results show that the dynamic performance of the armored servo is as anticipated and is comparable to the standard CH-54B servo. The servo completed the proof pressure test satisfactorily without showing any sign of permanent deformation or malfunction. The power consumption of the servo was within the limits set for the standard production servo, and the external leakage was acceptable. The internal leakage of the servo was within the limits set forth in the test plan except for the null leakage with the piston centered. The test plan called for a null leakage of 10 to 30 cc/min, which is in error. Actual leakage rates were 400 cc/min, which is realistic and acceptable for this unit. The forces required to move the servo input were as anticipated. The servo stroke was short of the design travel by 0.125 inch.

CONCLUSIONS

1. The function and response characteristics of the integral armored servo fabricated under this program are equivalent to those of the servo now operational on the CH-54B helicopter.

2. The integral armored servo provides a significant improvement in survivability as compared to the CH-54B servo with armor plate added. All flight-critical elements of the servo are protected from caliber .30 AP M2 ballistic projectiles with a velocity of 2750 feet per second.

3. The weight of the armored servo installation is considerably greater than that of the CH-54B servo with armor. Some of the weight differential can be attributed to the additional protection provided and some to the manufacturing techniques used for prototype manufacturing fabrication as compared to production techniques.

4. Other aircraft components which require armor shielding can be redesigned using DPSA integrated into the components. However, because of the limited shapes available, an increase in weight may result. True optimization can be achieved if the original design and installation consider the use of DPSA in its available forms, if the shapes and forms of DPSA are improved, and if the material technology is improved in the development of lighter weight DPSA.

5. In the stability analysis of the integral armored servo, it was found that the real parts of all roots were negative. Upon transformation, this results in a solution having only decaying exponentials, and it is thus concluded that the servo will be stable when operating in the flight control system.

6. Test results show that the integral armored servo performed in a manner similar to the CH-54B servo, and that servo performance is satisfactory.

APPENDIX I

STRESS ANALYSIS, ARMORED SERVO

LOADS

The servo is subjected to several different load conditions:

1. Dynamic flight loads.
2. Static operating loads.
3. Proof pressure loads.
4. Burst pressure loads.

Load categories 3 and 4 occur only during bench testing of the units. All loads are carried axially either in tension or compression. Side loads and moments cannot be transmitted to the servo through the mounting gimbal or the spherical output bearing. Internal stresses due to hydraulic pressure act only radially or axially.

Dynamic Flight Loads

The dynamic flight loads were obtained from CH-54B flight test data. For this analysis, only the most severe portion of the complete flight load spectrum was used. This portion corresponds to severe maneuvers at maximum gross weight and aft cg. These loads occur in the flight spectrum less than 10 percent of the time, making this analysis conservative. The seven most damaging load conditions are listed in Table I.

TABLE I. SERVO LOADS

Load Condition	F_S (lb)	F_V (±lb)
1	1750	4540
2	6830	2850
3	3020	2590
4	5660	1050
5	6120	1770
6	520	4590
7	4910	2870

Static Loads

Static operating loads can occur during ground check or system run-up. Neglecting the effects of the dead weight of the rotor head, the cylinder pressure corresponding to this condition is 1500 psi, which is the maximum possible servo null pressure. If the servo is driven against its internal stops during the ground check, full system pressure, 3000 psi,

may be present within the cylinder chambers. The maximum load corresponding to this pressure is

$$F = PA \qquad (1)$$

$$F = (3000) \times (3.53)$$

$$F = 10{,}600 \text{ lb}$$

If two stages are pressurized, the load increases to 21,200 lb.

Proof Pressure

Proof pressure loads occur only during bench testing. At this test the output is unrestrained; hence, all loads are internal. Internal pressures at proof are 150% of operating or 4500 psi, in accordance with MIL-H-5440, Hydraulic Systems, Aircraft, Types I and II, Design, Installation and Data Requirements For.

Burst Pressure

The burst pressure test is similar to the proof pressure test. Pressure is raised to 250 percent of operating pressure, or 7500 psi, in accordance with MIL-H-5440, Hydraulic Systems, Aircraft, Types I and II, Design, Installation and Data Requirements For. Permanent deformation is allowed, but no rupture of any component. Internal pressure at burst is 7500 psi.

CYLINDER BARREL (PART NUMBER 38650-11006)

The dimensions of both the first- and second-stage cylinder barrels are identical with the exception of the output rod shield on the first-stage barrel and the manifold attachment bracket on the second-stage barrel. The output rod shield on the first stage barrel is not a load-carrying member; therefore, it does not affect the analysis. The forces acting on the second stage barrel manifold attachment bracket due to the pressure forces acting on the transfer tubes are much smaller than the load forces acting on the barrel and are thus neglected.

TABLE II. DPSA PROPERTIES

	Inside	Outside
F_{tu}	250 ksi	300 ksi
f_{ty}	200 ksi	240 ksi
f_{cy}	250 ksi	300 ksi
f_{su}	100 ksi	150 ksi
E	30×10^6 psi	30×10^6 psi
W	.283 lb/in.^{3}	.283 lb/in.^{3}
S_{en}	70 ksi	70 ksi
S_{cn}	70 ksi	70 ksi

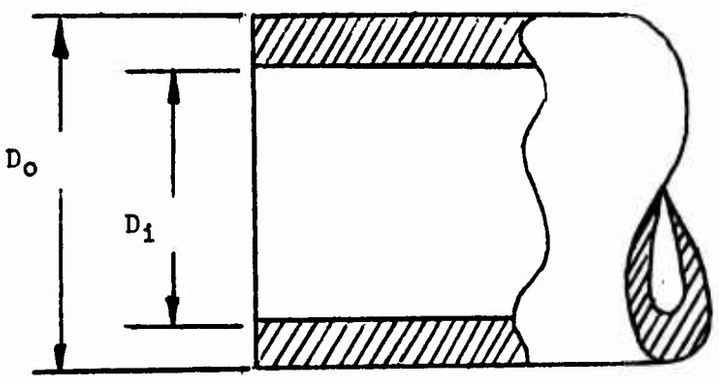

Figure 9. Barrel Dimensions.

Proof and Burst Pressures

The hoop stresses in the cylinder barrel are

$$S_{t(max)} = \frac{D_o^2 + D_1^2}{D_o^2 - D_1^2} P \qquad (2)$$

$$S_{a(max)} = \frac{D_o^2}{D_o^2 - D_1^2} P \qquad (3)$$

Substitution of numerical values yields

a. At P = proof pressure = 4,500 psi

$S_{t(max)}$ = 19,000 psi

$S_{s(max)}$ = 11,700 psi

b. At P = burst pressure = 7,500 psi

$S_{t(max)}$ = 31,600 psi

$S_{s(max)}$ = 19,500 psi

These values are well below the allowables; therefore, the barrels are adequate statically for proof, burst and operating pressures.

Radial Deflection Under Operating Pressure

The radial deflection is important in the design of hydraulic actuators. Radial deflection must be held to a minimum to insure proper sealing of the piston head seal against the cylinder wall.

The change in cylinder diameter is expressed as

$$\Delta D = \frac{S_t D_i}{E} \qquad (4)$$

At an operating pressure of 3000 psi, the change in diameter is

$$\Delta D_i = \frac{(12,650)(3.122)}{30 \times 10^6}$$

$$\Delta D_i = 0.00139 \text{ in.}$$

This increase in barrel diameter is well within the manufacturing tolerance for seal compression.

Stresses in the Barrel Retainer Groove

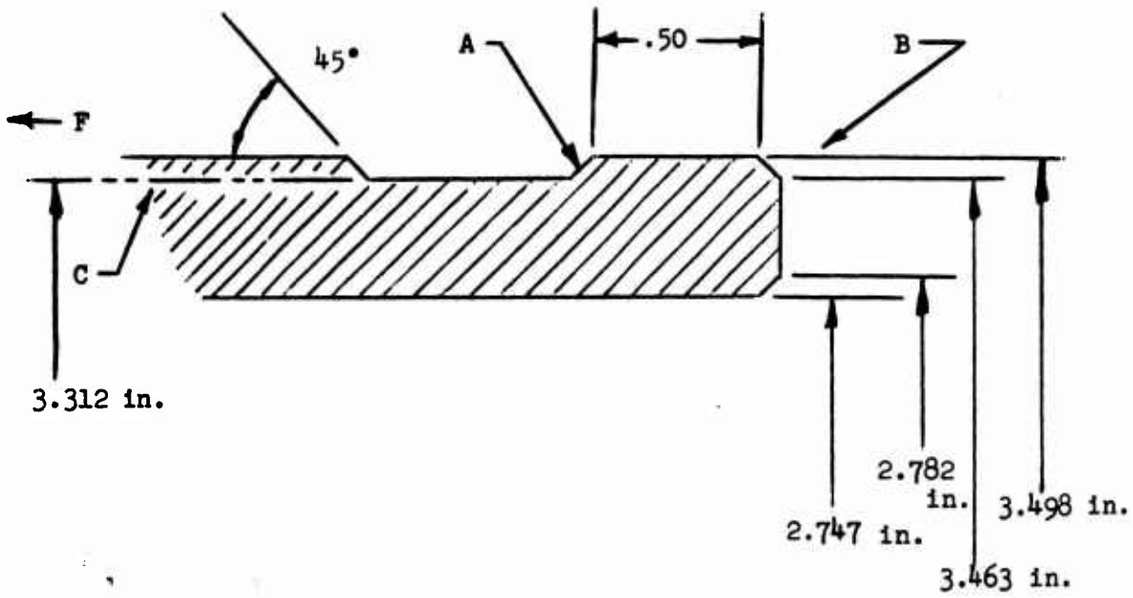

Figure 10. Barrel Retainer Groove.

(a) Bearing Area of Surface "A"

The bearing area "A" is 1.56 $in.^2$

The force acting on the area "A" is the force exerted by the locking dog due to the preload of the attachment bolts. This preload is made larger than the force exerted on this area by the internal pressures to prevent the barrel from lifting off the separator surface.

The maximum load due to bolt preload is 32,800 lb. The bearing stress, S_B, corresponding to this load is

$$S = P/A \qquad (5)$$

$$S = \frac{32{,}800 \text{ lb}}{1.56 \text{ in.}^2} = 21{,}000 \text{ psi}$$

This is well below the allowable bearing stress; hence, Area "A" is adequate in bearing. Stresses at area "B" will be treated in the analysis of the separator, which is of a softer material and therefore governs the size of area "B".

(b) Shear on Surface "C"

The depth of the undercut is sufficiently deep to place the shear area "C" into or below the diffusion zone between the inner and outer core of the barrel. Therefore, the strength of the inner core material must be used in evaluating the strength of this section.

The shear area is defined as

$$A_S = \pi DL \tag{6}$$

Substitution of numerical values yields

$$A_S = 5.2 \text{ in.}^2$$

By substituting into the basic stress equation (5), the shear stress along Section C is then found to be

$$S_S = \frac{32,800}{5.2} = 6,300 \text{ psi}$$

Therefore, the shear area "C" is adequate.

(c) Contraction of the Barrel in the Undercut

Contraction of the barrel takes place due to the influence of the normal forces developed by the locking dogs acting on the 45° slope. This force is at a maximum when the chamber adjacent to the undercut is unpressurized.

The normal force acting on the undercut has a value of

$$F_n = F/\sqrt{2} - F_u \tag{7}$$

$$F_u = (F/\sqrt{2})(u) \tag{8}$$

For steel with a surface finish of 32 RMS in sliding contact with a similar surface and assuming a thin oil film, the coefficient of friction μ is assumed to be .42.

Substituting into Equation (7),

$$F_n = 32,800 \left(1/\sqrt{2} - \frac{.42}{2}\right)$$

$$F_n = 13,350 \text{ lb}$$

This force acts on an area of 1.56 sq. in. The pressure is expressed by

$$P = F/A \tag{9}$$

Substituting into equation (9), the pressure is then 8550 psi. The stress on a cylinder subjected to external pressure is expressed as

$$S = \frac{2D_o^2 P}{D_o^2 - D_i^2} \tag{10}$$

Substituting into equation (10) yields

$$S = \frac{2(3.48)^2(8550)}{(3.48)^2 - (2.747)^2}$$

$$S = 45{,}000 \text{ psi}$$

The change in diameter resulting from this stress is established from equation

$$\Delta D = \frac{(2.747)(45{,}000)}{30 \times 10^6}$$

$$\Delta D = 0.00413 \text{ in.}$$

Since the diametral clearance is 0.006 in. minimum, no interference between the piston and cylinder will occur.

Fatigue Analysis of Barrel

The pressures and stresses corresponding to the flight loads assuming single-stage operation are listed in Table III.

TABLE III. SINGLE-STAGE LOAD-PRESSURE RELATIONSHIP

Load No.	Pressure (psi)	S_s (psi)	S_v (±psi)
1	495 ± 1,280	2,080	5,400
2	1,930 ± 810	8,150	3,420
3	855 ± 735	3,610	3,100
4	1,605 ± 297	6,770	1,250
5	1,730 ± 502	7,300	2,120
6	147 ± 1,300	620	5,480
7	1,390 ± 810	5,860	3,420

Quantitative data of DPSA fatigue characteristics are not available. The properties have been assumed to be similar to those of alloyed steel. The maximum allowable stress S_{en} for $K_t = 1$ is 67 ksi. We define the total small specimen reduction factor as

$$f_t = \frac{(f_s)(f_{su})(f_r)}{K_f} \tag{11}$$

The size factor, f_s, accounts for the reduction in mean endurance limit as the size of the component increases. Empirical data shows that the size factor is a function of the volumetric ratio of the component as compared to small specimens of approximately 0.3 in. in diameter with a volume of stressed material of 0.009 cubic in.

$$V_r = \frac{V}{0.009} \tag{12}$$

where V_r is the volume of the stressed part. Substituting

$$V_r = \frac{10.05}{0.009}$$

$$V_r = 1.115 \times 10^3$$

for this volumetric ratio, the size effect factor is 0.7.

The surface effect factor f_{su} is taken as unity. No test data is available on the effect of surface finish on material strength for DPSA. The reliability factor for a 3 sigma scatter is taken as $f_r = 0.7$.

For a smooth round barrel, the stress concentration factor K_f may be taken as unity. Substituting these values into Eq. (11), the total stress reduction factor is therefore found to be

$$f_t = \frac{(.7 \times (1) \times (.7)}{1} = .49$$

The maximum allowable vibratory stress for unlimited life thus becomes

$$S_{en} = (S_{en})(f_t) \tag{13}$$
$$S_{en} = 67 \times 0.49 = 32.83 \text{ ksi}$$

The modified Goodman diagram for unlimited life is shown in Figure 11.

From Figure 11, it is clear that the cylinder barrels are adequate in fatigue for all flight loads. This was anticipated since the barrels were designed for ballistic resistance rather than for endurance, and the ballistic requirement is more stringent.

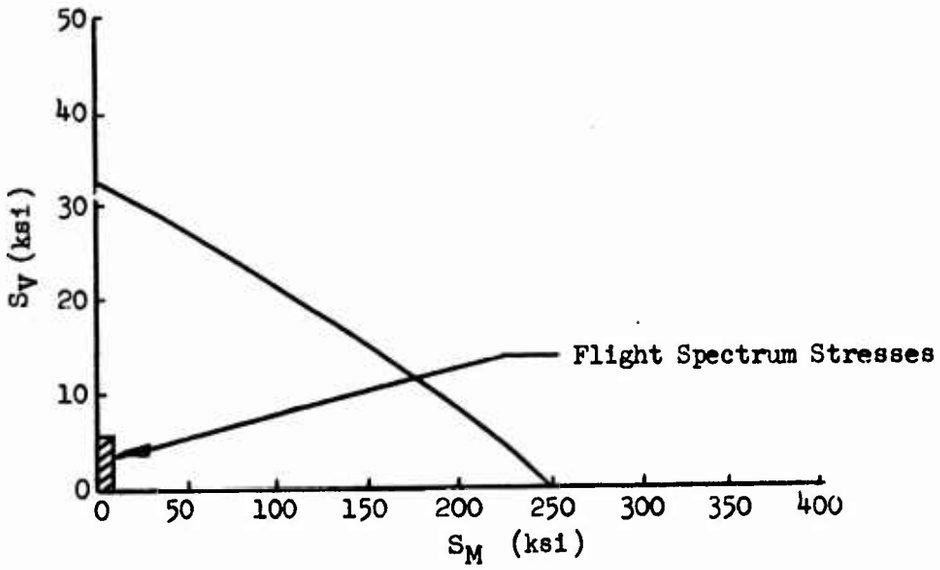

Figure 11. Goodman Diagram.

FIRST-STAGE PISTON (PART NUMBER 38650-11011)

The first-stage piston is machined from 17-4 PH stainless steel bar stock, heat treated to the H1025 condition.

The mechanical properties of 17-4 PH in the H1025 condition are shown in Table IV.

TABLE IV. PROPERTIES OF 17-4 PH CRES	
S_{tu}	150 ksi
S_{ty}	145 ksi
S_{cy}	145 ksi
S_{su}	94 ksi

The geometry of the piston is shown in Figure 12.

Section AA is the output rod end.

Section BB is the piston thread relief undercut.

Section CC is the piston head thread.

Section DD is the piston head thread chamfer.

Section E is the piston head face.

Section F is the seal gland.

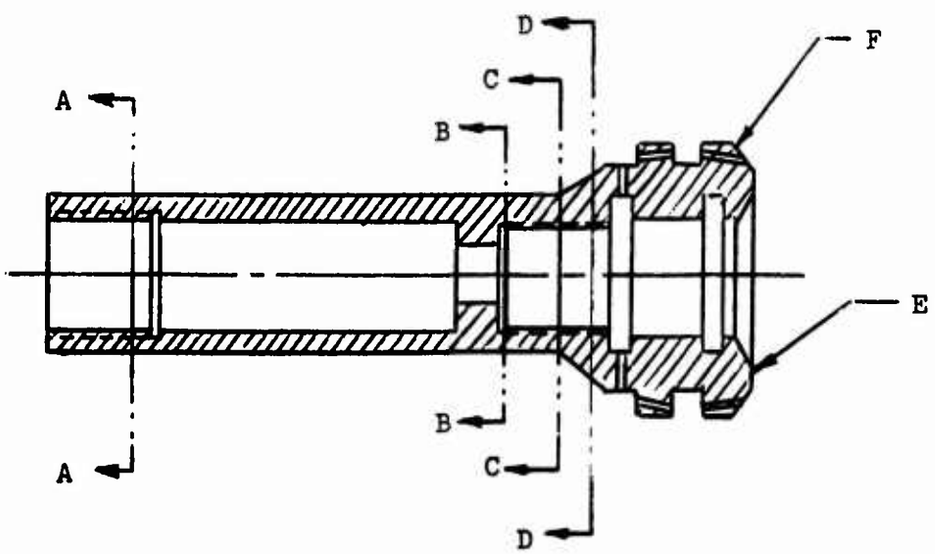

Figure 12. First-Stage Piston.

Output Rod End Thread Section AA

The load carried by the thread is the combined output force of the first- and second-stage outputs, the pilot effort and the output force of the auxiliary servo.

The servo output was found to be 21,200 lb.

The force due to pilot effort is taken as maximum pilot force times the control system linkage gain.

Maximum design pilot effort is 300 lb applied at the control stick. The linkage gain is found to be equal to 4.5; hence, total force equal to pilot effort is

$$F = 300 \text{ lb} \times 4.5 = 1{,}350 \text{ lb}$$

The auxiliary servo output is 460 lb; the resulting force of the servo output times the control system gain from auxiliary servo output to primary servo input is 490 lb. The total force seen at the output rod is therefore the sum of these forces, 23,040 lb.

1. Thread Preload

To prevent chafing of the rod end thread which can lead to early failure, the thread must be preloaded to a value above the maximum external load. Assuming a torque tolerance of 10 percent and using a maximum preload of 105% of maximum load, the preload becomes

$$F = 1.15 \times F_{max} = 26{,}500 \text{ lb}$$

The torque necessary to establish this preload is

$$T = F \times 0.2d \qquad (14)$$

for a thread diameter of 1.25 in.; the torque required to assure adequate preload is therefore 550 ft-lb.

The maximum load reacted by the rod end thread is then equal to the preload of the rod end.

2. Thread Shear and Tensile Area

The thread shear and tensile area was evaluated using the methods and formulae outlined in Screw Thread Standards for Federal Services, Handbook H28. The resulting shear and tensile areas of the thread were thus found to be

$$A_s = 3.299 \text{ in.}^2$$

$$A_t = 1.111 \text{ in.}^2$$

In considering the shear area, it is assumed that only one-third of the total thread engagement carries any load; therefore, the effective shear area is reduced to 1.1 $in.^2$. From equation (4), the stress is 24,500 psi.

The margins of safety are based upon a limit margin of 1.15 and an ultimate margin of 1.50. For the yield margin of safety, the margin is calculated as

$$MS = \frac{S}{1.15\ S_y} - 1 \qquad (15)$$

For the ultimate margin, the value is

$$MS = \frac{S}{1.50\ S_u} - 1 \qquad (16)$$

From equation (14), the shear margin of safety in yield becomes

$$MS = \frac{94,000}{1.15(24,500)} - 1 = +2.34 \quad \text{yield}$$

$$MS = \frac{94,000}{1.5(24,500)} - 1 = +1.55 \quad \text{ultimate}$$

Similarly, the tensile stresses can be calculated.

$$S_t = \frac{26,500}{1.11} = 23,800 \text{ psi}$$

The corresponding margins of safety are

$$MS = \frac{145,000}{1.15(23,800)} - 1 = +4.3 \text{ yield}$$

$$MS = \frac{150,000}{1.5(23,800)} - 1 = +3.2 \text{ ultimate}$$

3. Compressive Stress at the Rod End/Shaft Interface

The compressive force acting on the interface is the sum of the preload and the external force and is a maximum when the external force is compressive.

The maximum force is equal to

$$F = 26,500 \text{ lb} + 23,000 \text{ lb} = 49,500 \text{ lb}$$

The area over which this force must be reacted is .737 sq in.

The compressive stress in then found to be

$$Sc = \frac{49,500 \text{ lb}}{.737 \text{ in}^2} = 67,200 \text{ psi}$$

The corresponding margins of safety are

$$MS = \frac{145,000}{1.15(67,200)} - 1 = +.88 \text{ yield}$$

$$MS = \frac{150,000}{1.5(67,200)} - 1 = +.49 \text{ ultimate}$$

With a positive margin of safety, the bearing area is adequate for the loads imposed.

4. Fatigue Analysis of Thread

The stress concentration factor for a cut thread is estimated to be 4.45.

For this value of K_t, the value K_f is shown as a function of the frequency of occurrence in Table V.

TABLE V. K_f VALUES, PISTON THREAD

N(cycles)	K_f
10^4	1.6
10^5	1.85
10^6	1.9
$10^{7,8}$	1.95

The reliability factor is taken as $f_r = .7$ (alloy steels).

Assuming that only one-third of the total thread engagement carries load and that the stresses that are greater than .67 S_{max} occur only to a diameter of 1.45 in., we find that the stressed volume is

$$V = \pi/4\ (1.45^2 - 1.25^2) \times .6 = .254 \text{ in.}^3$$

The volumetric ratio is

$$V_r = \frac{.254}{.009} = 28.2$$

from which the size effect factor is $f_s = .8$.

The surface effect factor, f_{su}, is determined by the relationship of the strength of a part with a machined surface as compared to the strength of a similar part with a ground surface. For the piston, f_{su} is assumed to be .75.

Substituting into equation (11), the total strength reduction factor is

$$f_t = \frac{(f_r)(f_s)(f_{su})}{K_f} \qquad (11)$$

$$f_t = \frac{0.42}{K_f}$$

Based upon empirical data, the allowable stress for alloy steel with an S_{tu} of 150,000 psi and a ground surface is 60,000 psi. Using an allowable fatigue stress of 60,000 psi and the values of K_f from Table V, the value of S_{en} as a function of cycles has been calculated and is summarized and shown in Table VI.

TABLE VI. f_t AND S_{en} VALUES, PISTON THREAD

N	f_t	S_{en} (psi)
10^4	0.262	15,700
10^5	0.227	13,600
10^6	0.221	13,200
$10^{7,8}$	0.215	12,800

The Goodman diagram corresponding to these values is shown in Figure 13. The curves corresponding to 10^5 through 10^7 are omitted for clarity.

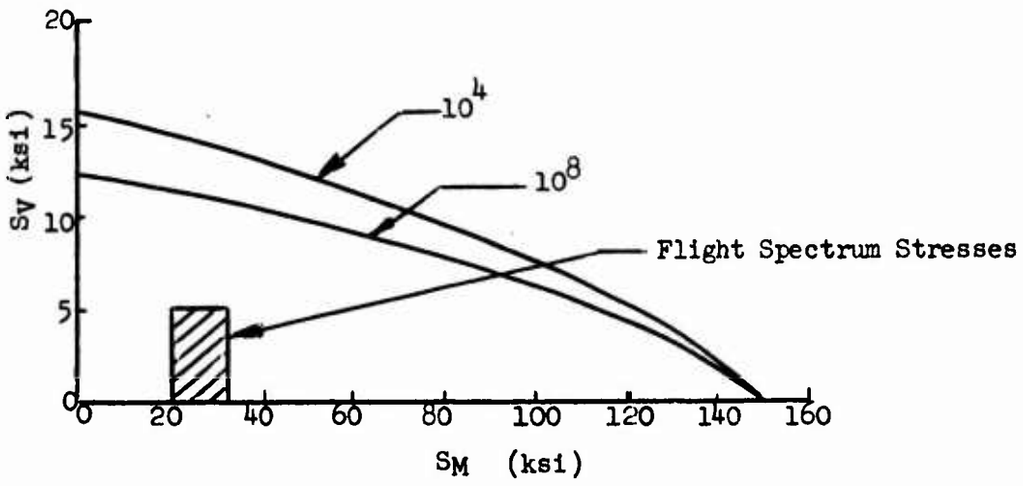

Figure 13. Goodman Diagram, Piston Thread.

Section BB

Section BB is taken through the piston head thread relief undercut. The load acting on this section is the combined output of the two stages, or 21,200 lb. The section area is 1.288 $in.^2$; from this, the stress in the section becomes 16,450 psi. The margin of safety for Section BB is then

$$MS = \frac{145,000}{1.15(16,400)} - 1 = +6.70 \text{ yield}$$

Section CC

The maximum load acting on this section occurs during the extend mode of the servo. At this time Section CC is subject to the combined output load of both stages and the preload of the threaded connection between the first- and second-stage piston. The preload between the first- and second-stage pistons must be greater than the maximum output capability of one stage. At P proof pressure, this force is equal to 15,831 lb. The torque selected is 300 ft-lb, which produces a preload force of 17,000 lb. The total load on the Section CC is then 17,000 + 21,200 lb = 38,200 lb. The section area is

$$A = \pi/4 \ (1.687^2 - 1.125^2) = 1.241 \text{ in.}^2$$

and the resulting stress is

$$S = \frac{38,200}{1.241} = 30,700 \text{ psi compressive}$$

The resulting margins of safety are

$$MS = \frac{145,000}{1.15(30,700)} - 1 = 3.11 \text{ yield}$$

$$MS = \frac{150,000}{1.5(30,700)} - 1 = 2.26 \text{ ultimate}$$

Section DD

Section DD is subjected to the same loads as Section CC. The section area is

$$A = \pi/4 \ (2.125^2 - 1.375^2) - 2(2.125 - 1.375)(.093) = 2.42 \text{ in.}^2$$

This is almost twice the area of Section CC, which is adequate. Therefore, Section DD is more than adequate statically.

Section EE

The maximum load occurring at Section EE is a compressive load due to the output of one stage and the piston preload. At P = P proof this force is equal to 33,000 lb. The area over which this force must be reacted is

$$A = \pi/4\ (1.71^2 - 1.437^2) - (1.71 - 1.437)(.19)$$

$$A = .553 \text{ in.}^2$$

The resulting stress becomes

$$S = \frac{33,000}{.553} = 59,700 \text{ psi}$$

The corresponding margins of safety are

$$MS = \frac{145,000}{1.15(59,700)} - 1 = +1.11 \quad \text{yield}$$

$$MS = \frac{150,000}{1.5(59,700)} - 1 = +.66 \quad \text{ultimate}$$

Therefore, Section EE is statically adequate.

Ultimate Static Strength

The maximum static load occurs at burst pressure. The most highly stressed section is Section EE. At burst pressure F = 43,500 lb , with the resulting stress of 78,500 psi. At this loading the margin of safety is

$$MS = \frac{150,000}{1.5(78,500)} - 1 = +.27 \quad \text{ultimate}$$

Therefore, the section is adequate under burst pressure test conditions.

Fatigue Analysis

1. Section BB

Treating the Section BB as a notched hollow shaft, K_t is assumed to be 2.9, f_{su} is .785 and f_s is .72 based upon a value of V_r of 14.8. Using a reliability factor of .7, we can now define the total stress reduction factor:

$$f_t = .396/K_f$$

Assuming a fatigue allowable stress of 60,000 psi, the allowable stresses as a function of N are shown in Table VII.

TABLE VII. K_f AND S_{en} VALUES, PISTON SECTION BB		
N	f_t	S_{en} (psi)
10^4	.240	14,400
10^5	.208	12,500
10^6	.188	11,300
10^7	.179	10,750
10^8	.176	10,600

The two loads of the load spectrum that have the highest steady and vibratory loads are

F_1 = 6,830 ± 2,850 lb

F_2 = 1,750 ± 4,540 lb

On the resulting stresses we superimposed a 40,000 psi compressive stress which is due to the shot peening. The final resulting stresses are

S_1 = 45,300 ± 2,210

S_2 = 41,360 ± 3,520

The Goodman diagram of Section BB is shown in Figure 14.

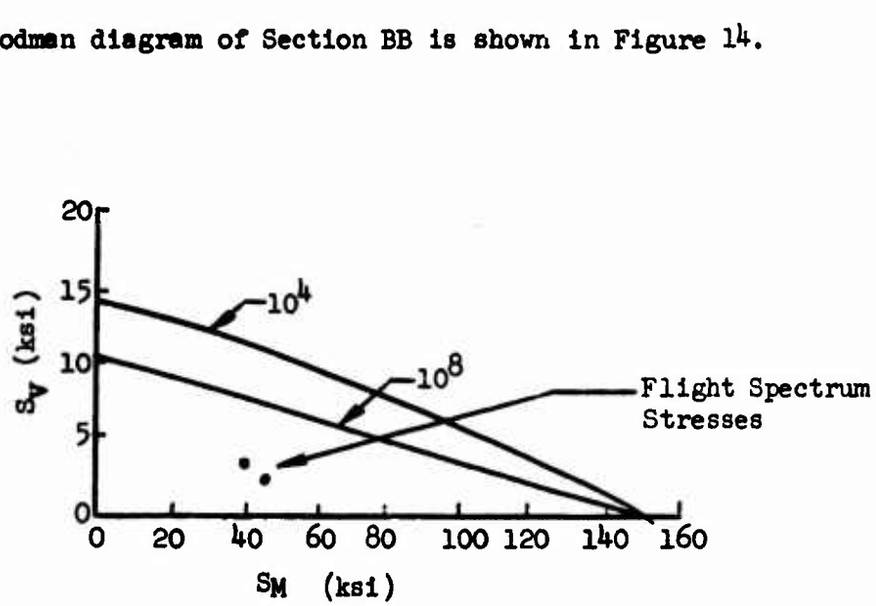

Figure 14. Goodman Diagram, Piston Section BB.

2. Section CC

Following the same procedures as for Section BB, we obtain the following parameters:

$K_t = 1.95$

$f_{su} = .785$

$f_r = .7$

$f_s = .8$

$f_t = .44/K_f$

The stress allowables are shown in Table VIII.

TABLE VIII. f_t AND S_{en} VALUES, PISTON SECTION CC

N	f_t	S_{en} (psi)
10^4	.293	17,600
10^5	.275	16,500
10^6	.275	16,500
$10^{7,8}$	.275	16,500

The total stresses in Section CC arise from the shot-peen stresses, preload stresses and flight load stresses. Using the same two flight loads as for Section BB, we obtain the two maximum stresses,

$S_1 = 59,300 \pm 2,300$ psi

$S_2 = 55,200 \pm 3,690$ psi

Figure 15 shows the Goodman diagram for Section CC.

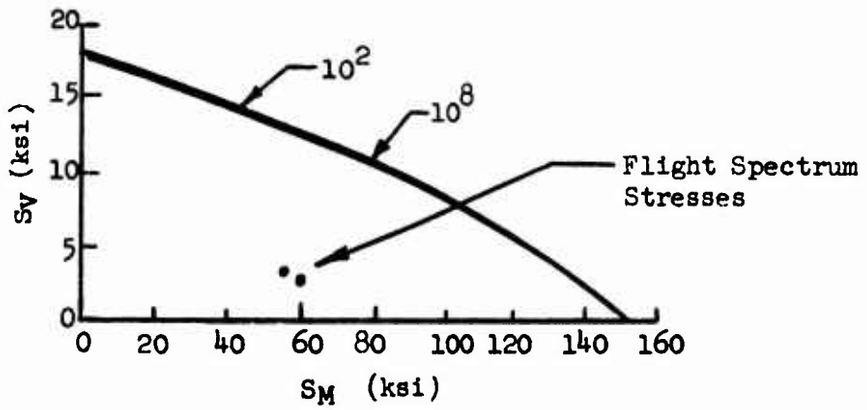

Figure 15. Goodman Diagram,
Piston Section CC.

3. Section DD

Section DD contains a stress riser in the form of the drilled oil passage. The following parameters are evaluated for this section:

$K_t = 2.43$

$f_{su} = .785$

$f_s = .785$

$f_r = .7$

$f_t = .432/K$

The allowable stresses as a function of N are shown on Table IX.

TABLE IX. f_t AND S_{en} VALUES, PISTON SECTION DD		
N	f_t	S_{en} (psi)
10^4	.278	16,650
10^5	.266	15,950
10^6	.264	15,800
$10^{7,8}$	.261	15,650

The loads acting on Section DD are equal to the loads at Section CC, but the resulting stresses at Section DD are approximately one-half the stresses at DD. Therefore, Section DD is adequate by analogy to Section CC.

4. Section EE

For Section EE we may take $K_f = 1$. The following parameters were evaluated for Section EE:

$f_r = .7$

$f_{su} = .785$

$f_s = .865$

$f_t = .475$

$S_{en} = 28,500$ psi

The stresses corresponding to the two maximum flight loads are

$S_1 = 83,200 \pm 5,120$

$S_2 = 74,000 \pm 8,200$

The Goodman diagram for the section is shown in Figure 16.

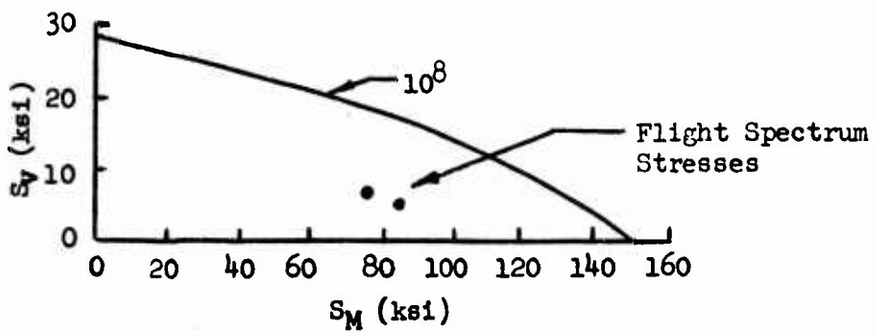

Figure 16. Goodman Diagram, Piston Section EE.

Servo Piston Head

1. Section F

This section is typical for both pistons. The servo piston head is subjected to the load exerted by the fluid pressure within the servo cylinder.

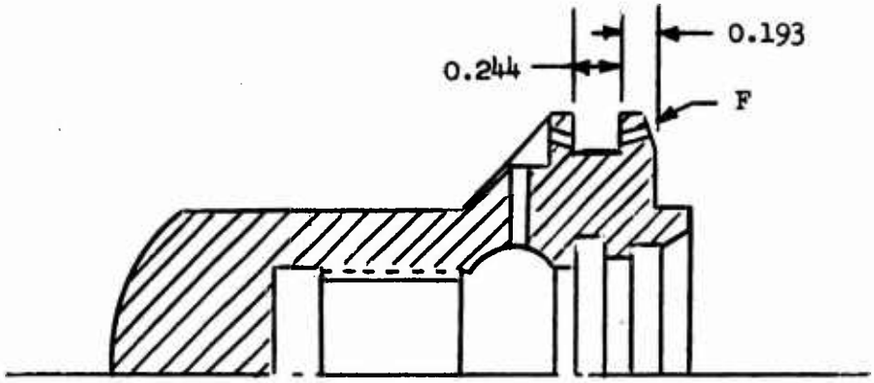

Figure 17. Piston Head Dimensions.

The shear area A_S is found to be

$$A_S = 1.61 \text{ sq in.}$$

The force acting on this area is the chamber pressure times the projected area of the seal groove. This area is

$$A = \pi/4 \ (2.75^2 - 2.373^2) = 1.54 \text{ sq in.}$$

At proof pressure, the shear stress in this section is then

$$S_S = \frac{4500 \times 1.54}{1.61} = 4300 \text{ psi}$$

2. Bending Stresses in Seal Groove

To calculate the bending stresses in the seal groove band, we let the pressure forces act through the centroid of the cross section. As a first approximation, the groove is assumed to be unrolled into a flat beam of length π d. This is conservative. The actual bending force in a true ring will be somewhat lower since the internal circumferential restoring forces that arise if the ring deflects under pressure are neglected. Taking a unit length slice of the section (see Figure 18), the moment of inertia of the cross-sectional area about its centroid is

$$I = .075 \text{ in.}^4$$

and the cg location is at C = .099 in. The stress due to bending is

$$S = \frac{(F)(C_1)(C_2)}{I} \qquad (17)$$

$$S = \frac{4,500 \times 1.54 \times 0.099}{.075}$$

$$S = 9,150 \text{ psi}$$

The total stress in Section F is

$$S = \sqrt{S_s^2 + S_b^2}$$

$$S = 10,100 \text{ psi}$$

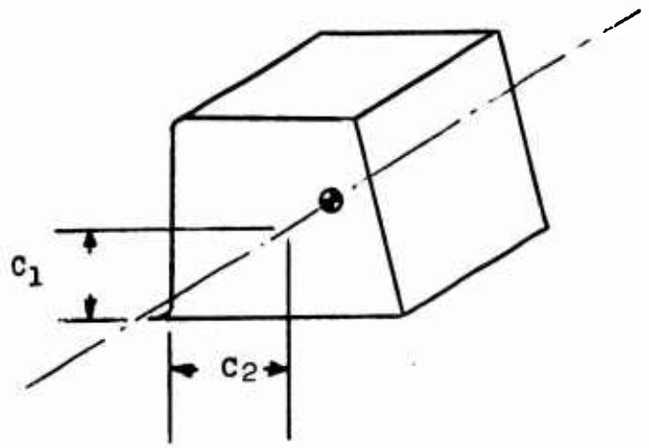

Figure 18. Seal Groove Dimensions.

This is well below the allowable for the piston material; hence, the piston head is considered adequate.

SECOND-STAGE PISTON (P/N 38650-11014)

The second-stage piston is machined from 17-4PH stainless steel bar stock, heat treated to the H1025 condition. The mechanical properties of this steel are listed in the first-stage piston analysis. The critical stress area of the second-stage piston is the end of the piston which mates with the upper piston. Figure 19 shows the cross section of this area.

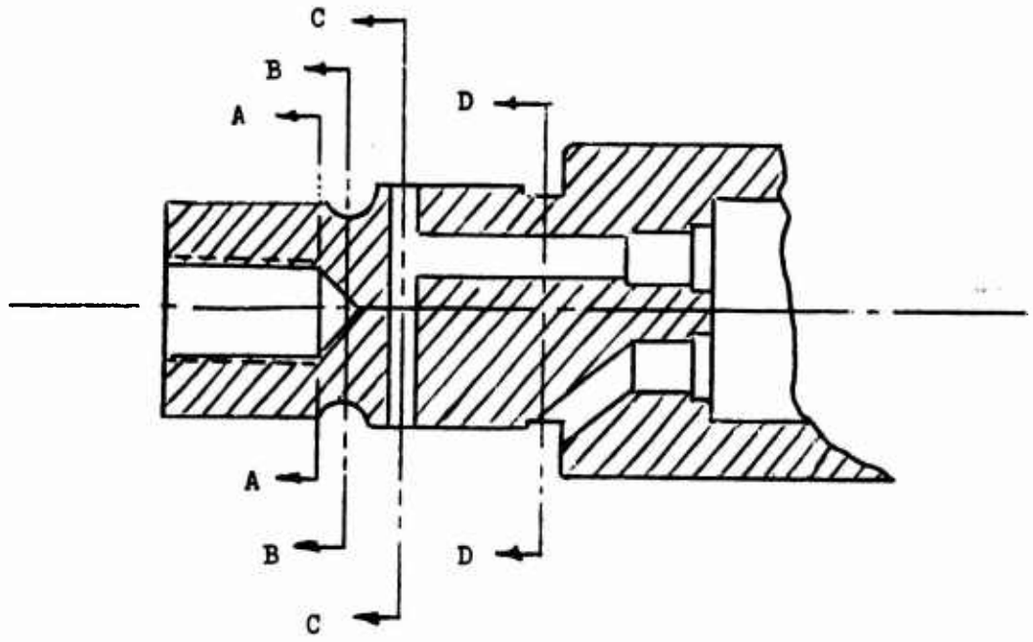

Figure 19. Second-Stage Piston.

Referring to Figure 19, we see that Sections AA through DD are subjected to the same loading. This load is the piston thread preload which puts Sections AA through DD into tension. The magnitude of the load is 17,000 lb.

Section AA

Section area is

$$A = \pi/4\ (1.0483^2 - .5^2) = .666\ \text{in.}^2$$

which results in a stress of

$$S_t = \frac{17,000}{.666} = 25,800\ \text{psi}$$

The resulting margins of safety are

$$MS = \frac{145,000}{1.15(25,800)} - 1 = +3.9 \quad \text{yield}$$

$$MS = \frac{150,000}{1.5(25,800)} - 1 = +2.8 \quad \text{ultimate}$$

Statically, Section AA is the weakest section; sections BB through DD have larger areas and are therefore not considered in the static analysis.

Fatigue Analysis

Sections AA through DD are not subjected to any fatigue loading. The preload on the piston thread is sufficiently high, such that any flight loads are not reacted through these sections. A fatigue analysis of these sections has been performed to study the fatigue strength of the piston end should the preload be zero. In all cases the analysis showed the piston to be good for at least 1×10^8 cycles. The details of the analysis will not be included in this report since it applies only to a hypothetical case.

PISTON ROD STRESS

Stresses in the piston rod are maximum directly adjacent to the piston head at Section AA.

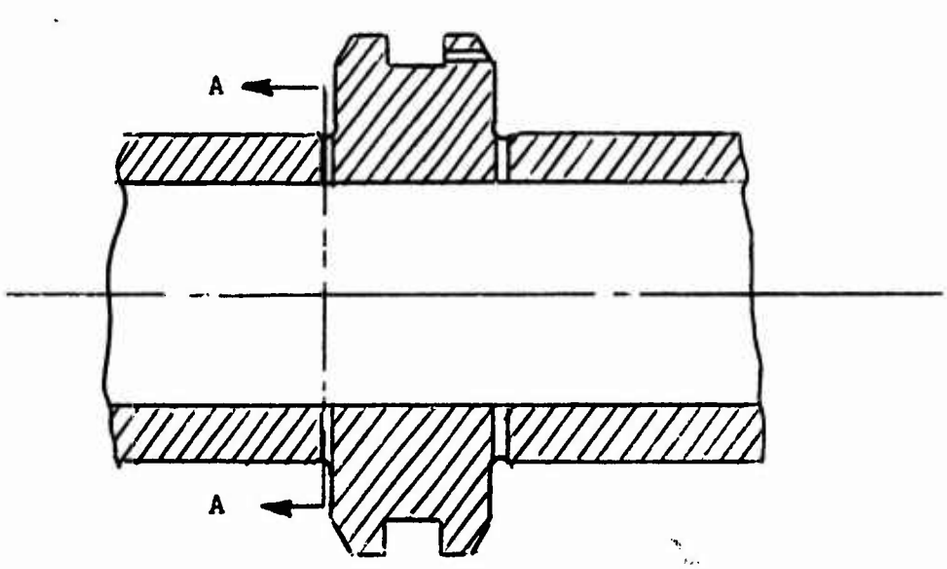

Figure 20. Piston Rod.

Section AA Static Stress

Section area $A = \pi/4\ (1.697^2 - 1.25^2) - 4(.093 \times .22) = .948$ in.^{2}. The maximum static load acting on this section is at proof pressure and is equal to 15,830 lb. The resulting stress is

$$S = \frac{15,830}{.948} = 16,730 \text{ psi}$$

The margin of safety is

$$MS = \frac{145,000}{1.15(16,730)} - 1 = +6.71 \text{ yield}$$

Fatigue Analysis, Section AA

Two stress risers are present at Section AA: the piston rod undercut and the oil transfer holes. The close proximity of the oil transfer holes to the undercut causes the stresses to peak approximately at the same point. The total stress concentration factor K_t is therefore the product of the individual stress concentration factor.

From the geometry of the undercut, the value for K_t is found to be equal to 1.8, and the K_t for the oil transfer holes is 3.1. The total K_t is

$$K_t = 1.8 \times 3.1 = 5.58$$

The values of the stress reduction factors are

$$f_r = .7$$

$$f_s = .78$$

$$f_{su} = .785$$

$$f_t = .43/K_f$$

Based upon an allowable fatigue stress of 60,000 psi, the allowable stresses as a function of N are listed in Table X.

TABLE X. f_t AND S_{en} VALUES, PISTON ROD

N	f_t	S_{en} (psi)
10^4	.226	13,550
10^5	.215	12,400
10^6	.21	12,600
$10^{7,8}$	.207	12,400

Conservatively assuming that only the second stage of the servo reacts the flight loads, the stresses in Section AA for the two most damaging loads become

$$S_1 = 47,200 \pm 2,330 \text{ psi}$$

$$S_2 = 41,850 \pm 4,800 \text{ psi}$$

The Goodman diagram for Section AA is shown in Figure 21.

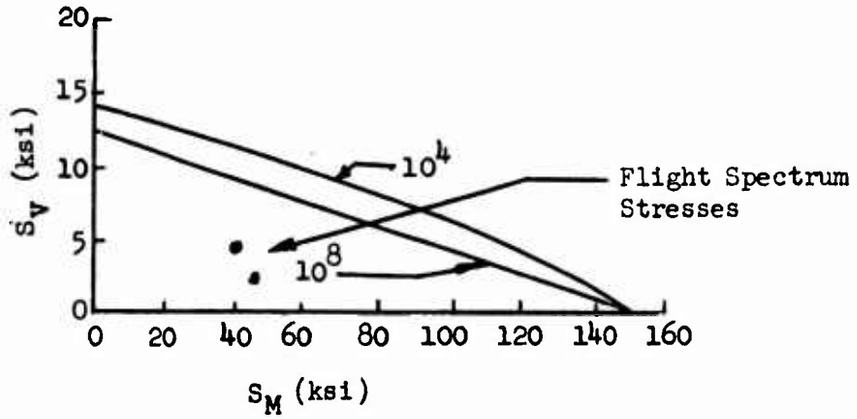

Figure 21. Goodman Diagram,
Piston Rod, Section AA.

The lower section of the second-stage piston is not subjected to flight loads. The only load acting on the lower half is the dead weight of the swash plate and push rods when the hydraulic system is turned off, or the force exerted by the fluid transfer tubes when the servo is pressurized. These forces are very much smaller than the flight loads. The mass of the rotating system acting on three servos is approximately 400 lb; hence, these loads are not considered. From the above analysis, the second-stage piston is found to be adequate to react the loads imposed on it.

OUTPUT ROD END (PART NUMBER 38650-11016)

The rod end is machined from 4340 bar stock.

Material properties, 4340 steel H.T. to 180,000 psi are

S_{tu} = 180 ksi

S_{ty} = 163 ksi

S_{cy} = 179 ksi

S_{su} = 109 ksi

The geometry of the rod end is shown in Figure 22.

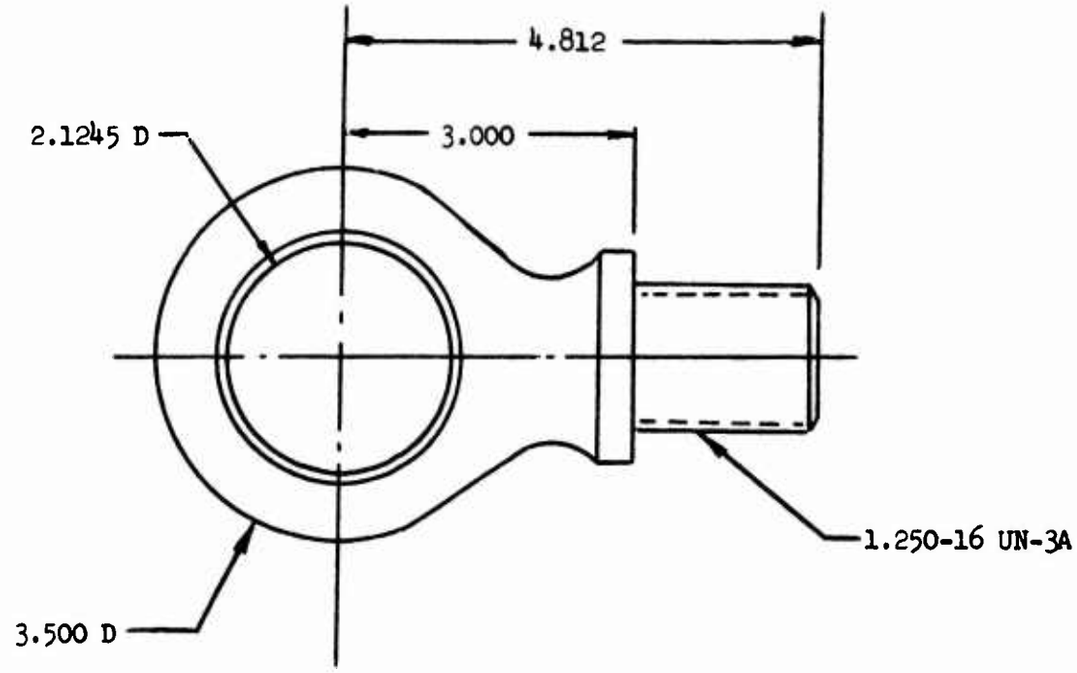

Figure 22. Output Rod End Dimensions.

Lug Analysis, Rod End

The allowable stress magnitude which can be imposed on a standard lug is defined by

$$S_{as} = S_{tu}\left(0.0338 + \frac{0.013}{(N \times 10^{-6})^{1/2}}\right) \qquad (18)$$

For a specific lug, the allowable stress magnitude becomes

$$S_{aa} = \left[\frac{1000 + 16.2\,(\text{Log } N)^4}{1000 + K_t(1+D)(2.7)(\text{Log } N)^4}\right](f_r)(S_{as}) \qquad (19)$$

These are empirical expressions based on data from a Royal Aircraft Establishment Technical Note No. Structure 182, January 1956, "The Strength of Lugs in Fatigue", by R. B. Heywood.

For a reliability of .7 and a K_t of 2.4, the allowable stress as a function of N is summarized below.

N	S_{aa}
10^4	16,600
10^5	6,450
10^6	4,120
10^7	3,240
10^8	3,060

The previously found values of S_{as} are valid for values of R, the ratio of minimum to maximum vibratory loads, equal to zero, which means the minimum applied load is zero. Taking tension loads as positive and compression loads as negative, we obtain a value of R particular to the CH-54 aircraft flight loads as equal to -.3. The slope of the R-line can be found from the relation

$$m = \frac{1 - R}{1 + R} \tag{20}$$

The angle ϕ that the R-line makes with the abscissa is then

$$\phi = \tan^{-1} (1 - R)/(1 + R) \tag{21}$$

Substituting numerical values yields $\phi = 29.5°$.

From Figure 18, the effective area of the lug is

$$A = (3.5 - 2.12)(1.25) = 1.72 \text{ in.}^2$$

The stress levels in the lug for the two most damaging flight loads, including a 40,000-psi steady stress due to shot peening, are

$$S_1 = 43,960 \pm 1,655$$

$$S_2 = 41,040 \pm 2,640$$

The Goodman diagram for the lug is shown in Figure 23.

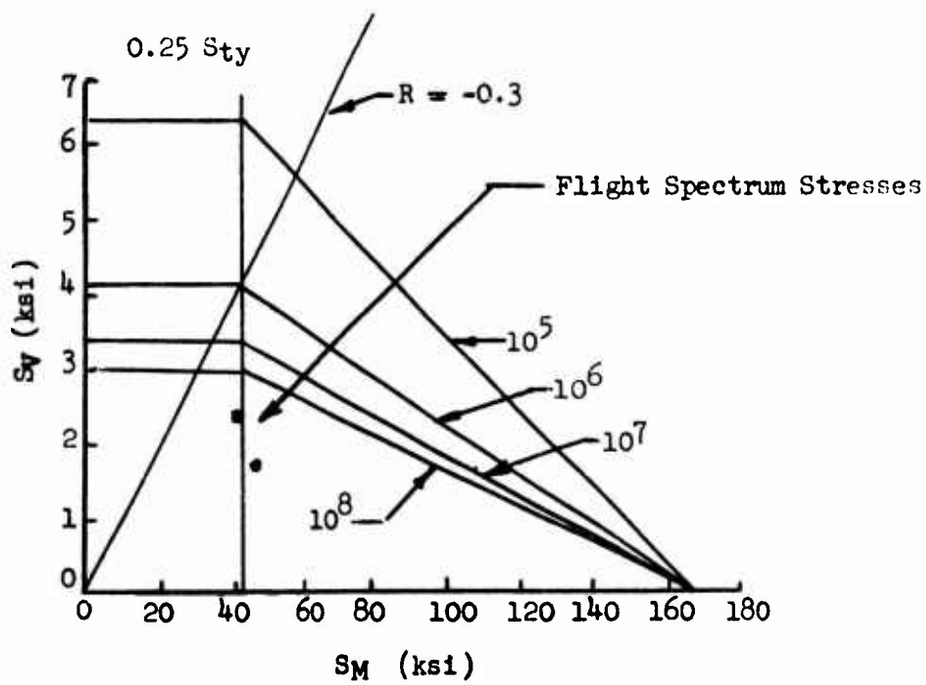

Figure 23. Goodman Diagram, Rod End.

Static Load Analysis

The maximum static load acting on the rod end is equal to the combined maximum output of the two servo stages, or 21,200 lb. The maximum stress in the lug corresponding to this load is 12,300 psi. This is about one-tenth of the maximum static allowable. Thus, statically the rod end lug is adequate.

Shank Section of Rod End

1. Static Stress

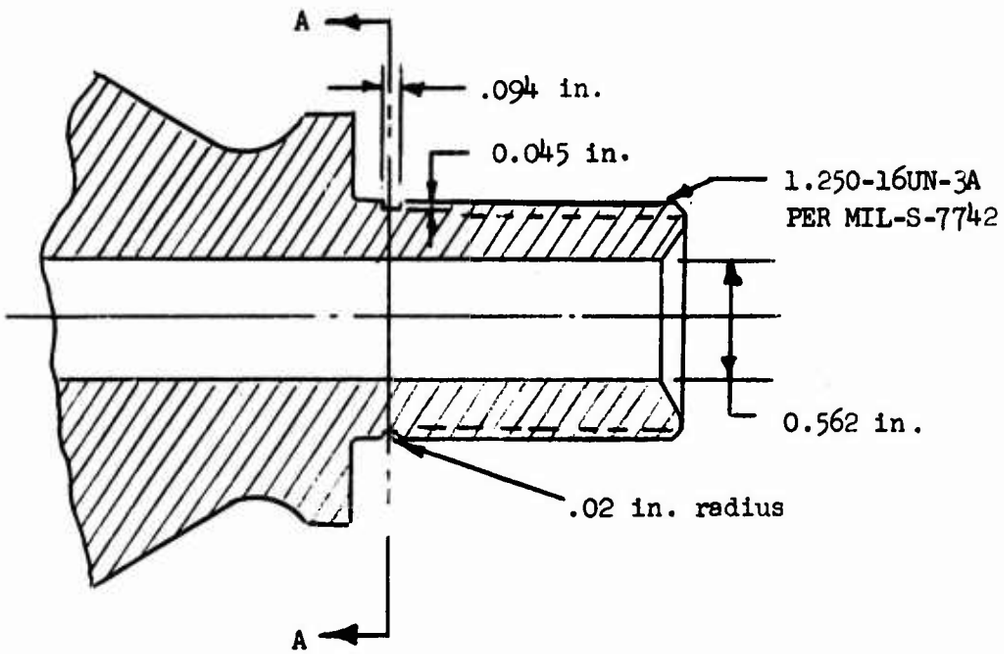

Figure 24. Rod End, Shank Dimensions.

The critical section of the shank as depicted in Figure 24 is Section AA.

The section area is

$$A = \pi/4\ (1.16^2 - .562^2) = .81 \text{ in.}^2$$

The load acting on this area is equal to the preload of the rod end which is 26,500 lb. The resulting stress in the section is then S = 32,700 psi, with a subsequent margin of safety of

$$MS = \frac{163,000}{1.15(32,700)} - 1 = +3.33 \quad \text{yield}$$

$$MS = \frac{180,000}{1.5(32,700)} - 1 = +2.67 \quad \text{ultimate}$$

2. Fatigue Analysis

Fatigue considerations are not applicable to this section. The thread preload does not permit any vibratory flight loads to appear at this section. An analysis was performed to study the case when the preload was zero, and the section was found to be adequate for the applied flight loads and to have unlimited life capabilities.

From the analysis, the rod end is adequate for all design loads.

Rod End Thread

No additional analysis is necessary to substantiate the integrity of the rod end thread. The thread was treated in the upper piston analysis and found to be adequate for the lower strength material of the piston.

Separator (Part Number 38650-11013-2)

The separator is designed to perform several functions which influence the loadings to which it is subjected:

1. Separate the two hydraulic systems.
2. Act as a base against which the two cylinder barrels are
3. Provide a load path between the servo and the gimbal assembly.

The interior sections of the separator are subjected only to fluid pressure. This results in a loading of 7500 psi maximum at burst test. This is well below the compressive strength of the material and need not be considered. Bearing stresses occur at the section where the cylinder barrel contacts the separator. The magnitude of this loading is a function of the bolt preload of the assembly. Bearing stresses also occur at the gimbal pin bearings. These stresses are treated in the analysis of the pin bushings, since the stresses in the bushing are more critical. Bending stresses are not considered. The preload on the barrel separator interface is in excess of any external loads acting on the servo, precluding any deformation due to the out-of-phase loading of the gimbal structure.

The separator is machined from 17-4PH stainless steel, heat treated to the H1025 condition.

Bearing Stress

The total preload of the barrel retaining bolts is equal to 32,800 lb. The bearing area is 2.995 $in.^2$. The compressive stress of that area is therefore 10,950 psi. This stress is less than 10% of the ultimate strength of the material. The bearing area is therefore considered adequate.

LOCK RING (PART NUMBER 38650-11012)

The lock ring is machined from 4340 alloy steel heat treated to 180000 psi. The lock ring is subjected to both shear and bearing loads. A cross section of the lock ring is shown in Figure 25.

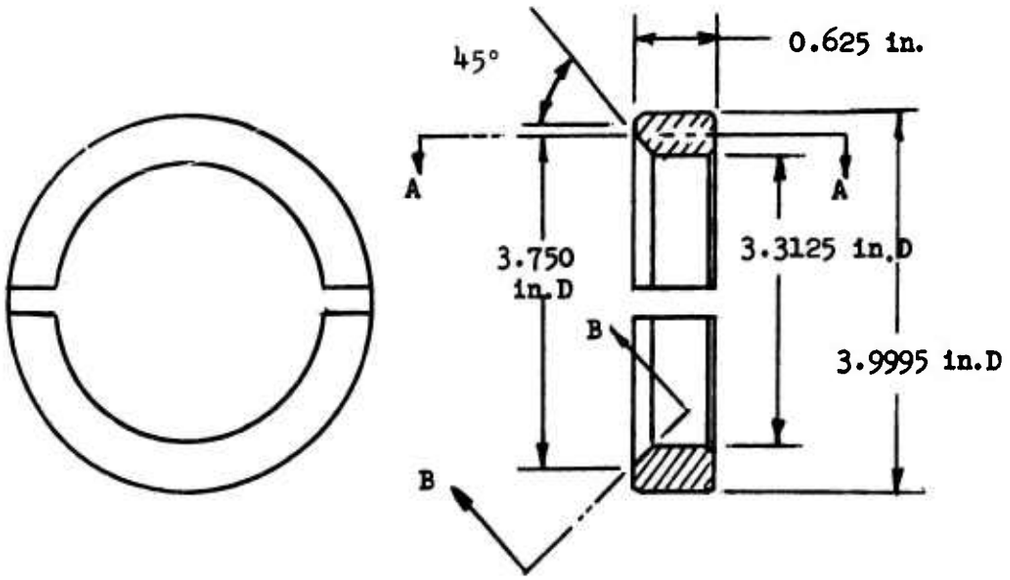

Figure 25. Lock Ring Dimensions.

1. Shear Stress

The maximum shear occurs along line AA. The load on the lock ring is equal to the preload of the retaining bolts, which is 32,800 lb. The shear area is A_s = 7.66 $in.^2$. The shear stress resulting from this is 4280 psi, which is negligible.

2. Bearing Stress

The maximum bearing loads are reacted at Section BB. The area of Section BB is 1.406 in. For a loading of 32,800 lb, the bearing stress becomes 23,300 psi. The margin of safety of Section BB

is

$$MS = \frac{179,000}{1.5(23,300)} - 1 = +4.12 \text{ ultimate}$$

Therefore the lock ring is adequate to carry all static loads. Vibratory loads are eliminated from the lock ring due to the high preload of the barrel retaining ring bolts.

UPPER AND LOWER RETAINING RING (PART NUMBER 38650-11012-2, -3)

The retaining rings are machined from 4340 alloy steel bar stock and heat treated to 180,000 psi. The major structural dimensions are common to both rings. In addition, the loads carried by each ring are identical. For this reason, only one ring has been analyzed, and the results are applicable to the other except where differences occur, such as the threads in the lower housing. The basic structural shape common to both members is shown in Figure 26.

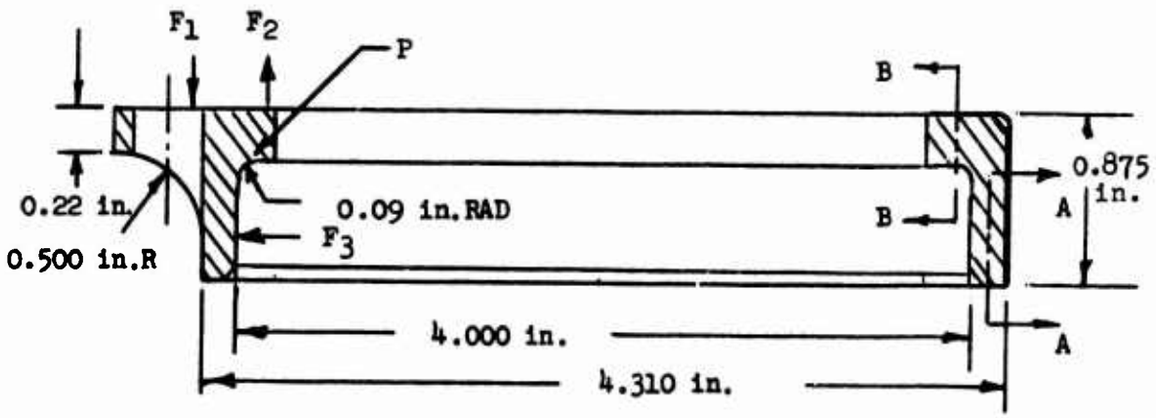

Figure 26. Retaining Ring Dimensions.

The stress occurring in the section shown in Figure 26 is composed of several components: an axial component due to the compressive force on the lock ring, a radial component due to the outward force of the lock ring, and a bending moment due to the retaining bolts.

BEARING STRESS

The bearing stress on Section BB is equal in magnitude to the lock ring bearing stress. Its value is S = 18,300 psi.

Shear Stresses in Section AA

The load acting on Section AA is 32,800 lb, which is the lock ring reaction force. The shear area along Section AA is 2.76 $in.^2$. The shear stress is then 11,900 psi and the corresponding margin of safety is

$$MS = \frac{109,000}{1.5(11,900)} - 1 = +5.1 \quad \text{ultimate}$$

Radial Stress

This stress is a hoop stress set up in the returning ring as a result of the outward pressure of the lock ring on the retainer. The hoop stress for a thick-walled cylinder is defined by

$$S = \frac{D_o^2 + D_i^2}{D_o^2 - D_i^2} \; P \qquad (22)$$

Substitution of the retaining ring dimensions yields S = 13.3 P. To evaluate the pressure P, we recall from the barrel analysis a compression force acting on the barrel retaining undercut of 23,100 lb. This force must be reacted by the retaining ring over an area of 8.23 $in.^2$. The resulting equivalent pressure force then becomes 2,810 psi, from which the hoop stress then becomes S = 37,300 psi.

Bending Stress

Taking section through the retaining ring at a bolt hole location, we can establish the moment of inertia of that section about its cg by summing the moments of inertia of the individual sections. Refer to Figure 22 for the section details.

The cg location of the composite section is at coordinates X = .6083 and y = .5968. The section moment of inertia about the cg is I = .011154 $in.^4$. The force F_1 is the retaining bolt force, F_2 is the lock ring axial force, and F_3 is the lock ring radial force. The total moment of these forces about the cg is the sum of these moments. By definition, $F_1 = -F_2$, since F_2 is the reaction force of the bolt preload F_1. The resulting moment about the cg is 2,980 in.-lb. The stress at point P in Figure 26, corresponding to this moment is 15,600 psi. The maximum stress at point P can be evaluated using the technique of stress at a point. For small deformations we may write the expression for the principal stress:

$$\begin{vmatrix} \sigma_x - \sigma & \tau_{xy} \\ \tau_{xy} & \sigma_y - \sigma \end{vmatrix} = 0 \qquad (23)$$

Solving this relation for σ_1 and σ_2, the two principal stresses

$$\sigma_1, \sigma_2 = \frac{\sigma_x + \sigma_y}{2} \pm \frac{(\sigma_x - \sigma_y)^2}{4} + \tau_{xy}^2 \qquad (24)$$

Substitution of numerical values into the above relation yields

$$\sigma_1 = 55{,}350 \text{ psi}$$

$$\sigma_2 = 15{,}850 \text{ psi}$$

The maximum stress σ_1 results in an ultimate margin of safety:

$$MS = \frac{180{,}000}{1.5(55{,}350)} - 1 = +1.16 \text{ ultimate}$$

The retaining ring is therefore adequate.

Threads in the Lower Retaining Ring

The thread depth exceeds the thread depth of standard MS21045 nuts, which are rated at 14,500 lb tension load. Each thread in the retaining ring is subjected only to a tensile load of 4,200 lb.

Retaining Ring Fatigue Analysis

The preload on the retaining ring prevents any vibratory loads of the flight load spectrum from appearing in the retaining ring. Therefore, fatigue considerations are neglected. A check was performed to establish the component life in case of a preload loss, and the retaining ring was found to be adequate for infinite life when subjected to flight loads.

PIN, TRUNNION PIVOT (PART NUMBER 38650-11013-3)

The trunnion pin is machined from 9310 alloy steel, carburized to a case hardness of Rockwell C58-64 and a core hardness of Rockwell C30-45.

For the analysis, only the strength of the core material is considered. The core material properties are

$$S_{tu} = 130 \text{ ksi}$$

$$S_{ty} = 115 \text{ ksi}$$

$$S_{cy} = 127 \text{ ksi}$$

$$S_{su} = 87 \text{ ksi}$$

Figure 27 illustrates the geometry of the pin.

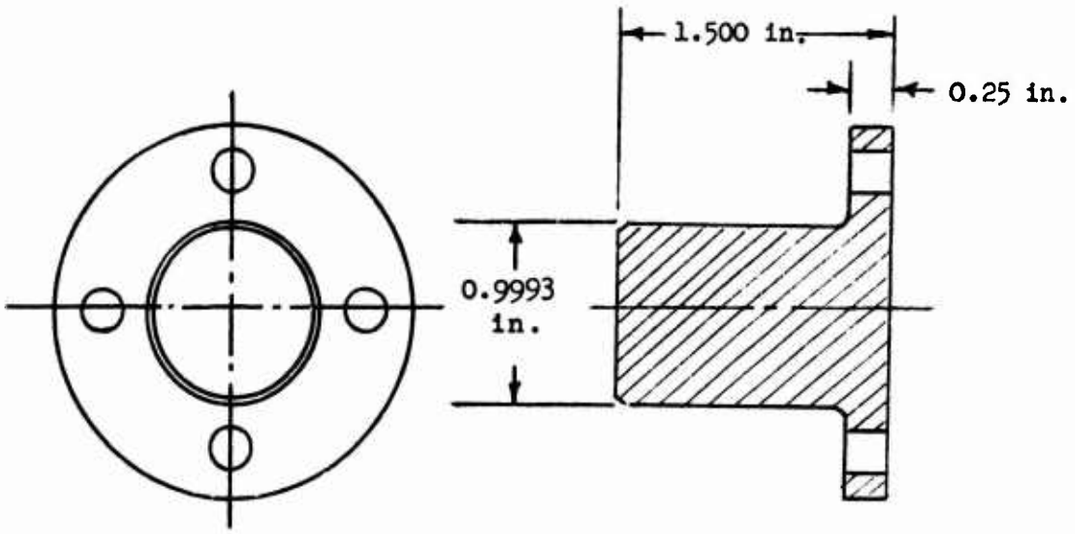

Figure 27. Trunnion Pivot Pin Dimensions.

Static Analysis

The maximum static load reacted by the pin is the combined output of both stages at operating pressure, and the output is restrained. Burst and proof pressure loads are not reacted through the pins. Forces generated in the auxiliary servo and pilot control forces are reacted through the piston rod and are not felt at the trunnion.

The maximum load, F, is 2 x 10,600 lb = 21,200 lb. It is assumed that the load is shared equally between the two pins, and each pin is subjected to a load of 10,600 lb. This load sets up bearing, shear and bending stresses in the pin. After the initial yielding of the local high spots and the initial wear in of the pin in the bushing, the bearing area is conventionally taken as the product of the pin diameter times the length of the bushing. Taking a conservative approach, we assume the bearing area to be one-half of that value or .31 $in.^2$. The resulting bearing stress then is 34,200 psi.

The shear area of the pin is .7854 $in.^2$, resulting in a shear stress of 13,500 psi.

A bending moment arises from the separation of the applied load and the reaction force. From the geometry of the pin and the load magnitude, this moment is evaluated to be 9,400 in.-lb. The moment of inertia of the pin cross section is .7854 $in.^4$; therefore, the stress at the extreme fiber of the pin is 6,000 psi. The margin of safety for combined stresses is given

by

$$MS = \frac{S_{ty}}{1.15\sqrt{(S_t + S_b)^2 + (2S_s)^2}} - 1 \quad \text{yield} \tag{25}$$

$$MS = \frac{1}{1.5\sqrt{\left(\frac{S_t}{S_{tu}} + \frac{S_b}{S_{bu}}\right)^2 + \left(\frac{S_s}{S_{su}}\right)^2}} - 1 \quad \text{ultimate} \tag{26}$$

Substitution of numerical values yields

$$MS = 2.28 \quad \text{yield}$$

$$MS = 1.96 \quad \text{ultimate}$$

which assures that the pin is adequate in static applications.

Pin Fatigue Analysis

Each pin is subjected to one-half of the applied flight loads. The maximum allowable stress for the core material is S_{en} = 55.5 ksi. The stress concentration factor K_t for the pin is unity. The surface effect factor f_{su} is unity. The reliability factor is taken as f_r = .7, and the size effect factor f_s = .85. The total reduction factor is then f_t = .595, which results in a S_{en} = 33 ksi.

The Goodman diagram for the pin is shown in Figure 28.

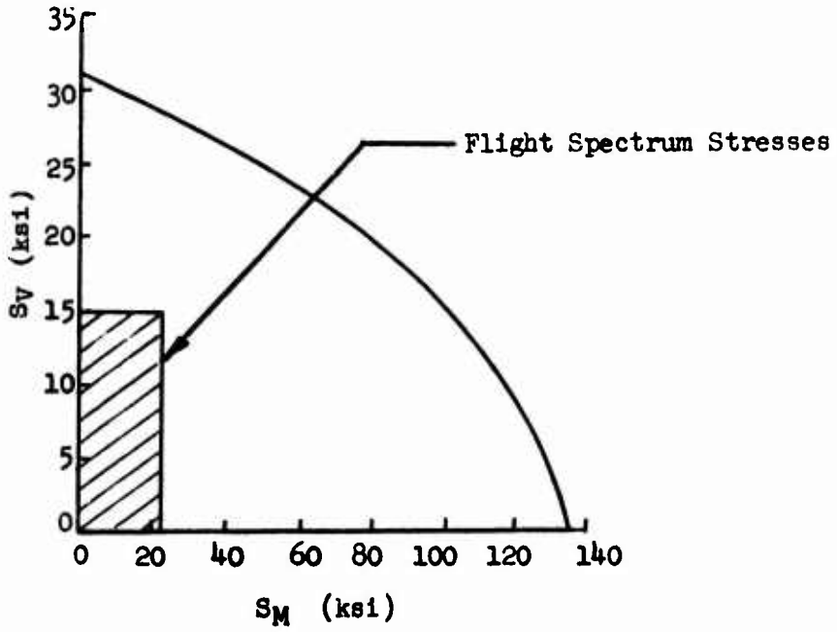

Figure 28. Goodman Diagram, Trunnion Pivot Pin.

END CAP (PART NUMBER 38650-11013-5, -6)

The end cap is machined from 7075 AL in the T73 condition. The properties for this material are

S_{tu} = 77 ksi

S_{ty} = 66 ksi

S_{cy} = 64 ksi

S_{su} = 46 ksi

The end cap sees the same pressure as the piston head. Therefore the maximum static load on the end cap is a burst pressure, or 26,500 lb. For the critical area, which is the thread, we must add the load due to the end cap torque. This torque results in an additional load of 11,000 lb. Therefore, the maximum load reacted by the end cap threads is 37,500 lb.

Static Analysis of End Cap Thread

For the 2.875-16UN3A thread we have a shear area of A_s = 2.66 in.^{2} and a tensile area of 6.2 in.^{2}. The corresponding stresses at burst pressure are

S_s = 14,100 psi

S_t = 6,000 psi

The margin of safety for the shear stress, which is the critical stress, is

$$MS = \frac{46,000}{1.5(14,100)} - 1 = 1.17 \text{ ultimate}$$

The end cap thread is therefore adequate statically for maximum loads.

Fatigue Analysis of End Cap

For fatigue loading, the end cap thread is the critical area due to the high stress concentration inherent in a cut thread. Further, the thread preload and cylinder pressure loads combine at the piston thread; conversely, at the end cap flange, the thread preload and the cylinder pressure loads substract.

Thread Analysis

The value of K_t for a cut thread is found to be equal to 4.45. The corresponding value of K_f as a function of N is shown in Table XI.

The reliability factor of the aluminum alloy, f_r, is 0.61.

The size effect factor is evaluated from the volumetric ratio of the stress volume that is stressed at .67 S_{max} (or more) to the test specimen volume. The stress volume can be found from the relation

$$.67\ S_{max} = P/.7854\ (D_o^2 - D_i^2) \qquad (27)$$

where D_i is the inner diameter of the end cap in the thread area and D_o is the diameter sought. Substitution of numerical values into Equation 19 yields $D_o = 2.52$ in. The stressed volume then is .613 $in.^3$, yielding a volumetric ratio of 68, which then leads to a size effect factor of $f_s = .715$. The surface effect factor f_{su} for the machined thread is .92. The total reduction factor then becomes $f_t = .4/K_f$.

The allowable stresses are given in Table XI.

TABLE XI. ALLOWABLE STRESS VS. N

N	K_f	f_t	S_{en}
10^4	2.8	.143	7,850
10^5	3.0	.1335	5,350
10^6	3.15	.127	3,560
10^7	3.3	.1215	2,920
10^8	3.3	.1215	2,680

The Goodman diagram is given in Figure 29 for the values of S_{en} given in Table XI. The curves corresponding to 10^5 to 10^7 cycles are omitted for clarity.

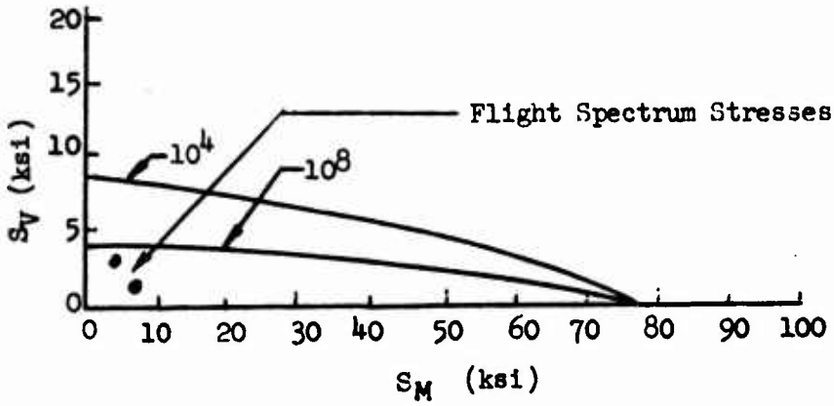

Figure 29. Goodman Diagram, End Cap.

From the Goodman diagram, it can be seen that the end cap is adequate in fatigue.

MANIFOLD (PART NUMBER 38650-11015-1, -2)

The manifold is machined from 2024-T351 aluminum bar stock. The properties for this material are

S_{tu} = 62 ksi

S_{ty} = 40 ksi

S_{cy} = 32 ksi

S_{su} = 37 ksi

The primary function of the manifold is to provide a link between the stationary pressure input and the moving valve body. As this, the manifold provides the sealing arrangement for the transfer tubes. Stresses occur within the manifold only with system pressure. Forces due to transfer tube seal friction and the transfer tube unbalanced pressure forces are small and may be neglected. Vibratory load pressures are not present in the manifold. Fatigue considerations are valid only for system "On-Off" cycles.

Static Stresses

The manifold is assumed to be similar to a thick walled cylinder of uniform cross section. By using the narrowest portion of the manifold cross section as the outside diameter of the hypothetical cylinder, considerable conservatism is built into the analysis. Figure 30 illustrates the method used for analysis.

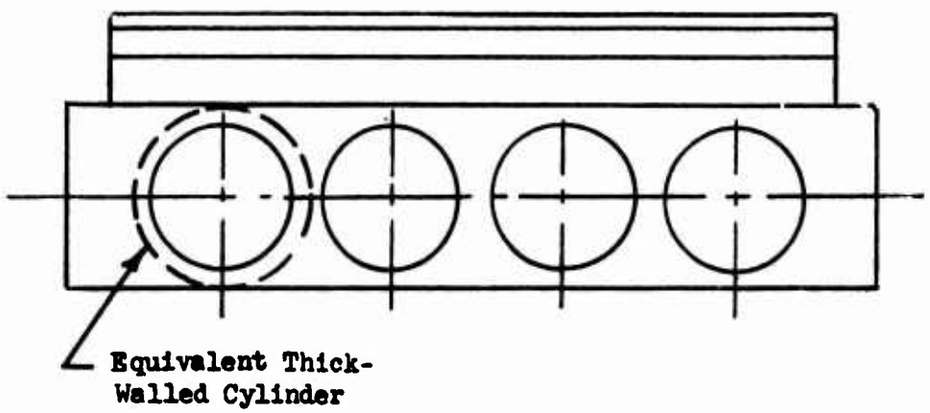

Figure 30. Manifold Dimension.

The cylinder C is subjected to an internal pressure P_i. The maximum stress in this cylinder occurs at the inside radius and can be evaluated from the equation

$$S_{max} = P_i\left(\frac{D_o^2 + D_i^2}{D_o^2 - D_i^2}\right) \qquad (28)$$

Substitution of numerical values yields

at P_i = 3,000 psi S_m = 5,800 psi

P_i = 4,500 psi S_m = 8,700 psi

P_i = 7,500 psi S_m = 14,500 psi

The resulting margins of safety for P_i = 7,500 psi are

MS = 1.39 yield

MS = .835 ultimate

Fatigue Analysis

A low-cycle, high-stress condition exists in the manifold during sytem "On-Off" operation.

For the manifold, assume a K_t of unity. The surface is considered in the machined condition, yielding an f_{su} = .725. The reliability factor f_r for aluminum is taken as .61. By evaluating the stressed volume in the established manner, we arrive at a value for f_s = 0.73. The total reduction factor is evaluated to be f_t = .323. The maximum stress allowables as a function of N are given in Table XII.

TABLE XII. ALLOWABLE STRESS VS. CYCLES, MANIFOLD

N	S_{en}
10^5	9,450
10^6	7,850
10^7	6,850
10^8	5,500

Pressure within the manifold bore results in a shear force at the bore end. The area in shear is 0.222 sq in. At 3,000 psi hydraulic pressure, the force is 745 lb, and the stress is 3,360 psi.

The Goodman diagram is given in Figure 31. The curve for 10^6 cycles has been omitted for clarity.

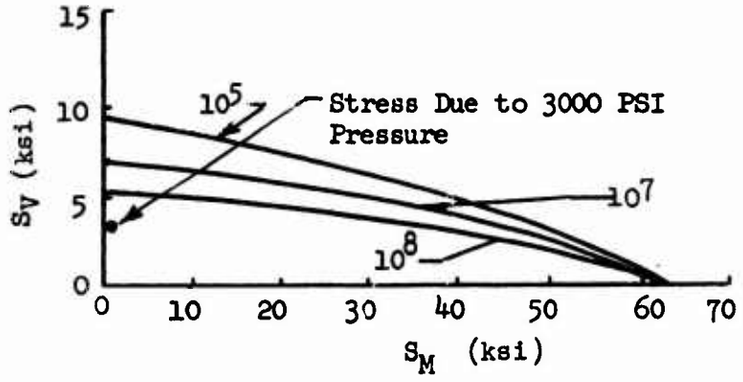

Figure 31. Goodman Diagram, Manifold.

From the Goodman diagram, it can be seen that the manifold has a life limited to 10^7 cycles when subjected to 3,000 psi pressure variations. The standard criterion is that there are 10 "On-Off" cycles per aircraft flight hour. This relates to a service life of 10^6 flight hours for the manifold, which is more than adequate.

Rod, Oil Transfer (Part Number 38650-11015-3)

The rod is machined from 17-4PH stainless steel, heat treated to the H1025 condition.

The transfer rods are subjected to the same load spectrum as the manifold and are subjected only to supply pressure.

Static Analysis

Treating the rod as a thick walled cylinder, the hoop stress becomes $S = 1.98\ P$. Substitution of values for P at operating, proof and burst pressure yields values of stress equal to 5,950, 8,940 and 14,850 psi respectively. The ultimate margin of safety then becomes

$$MS = \frac{150,000}{1.5(14,850)} - 1 = +5.74 \quad \text{ultimate}$$

Hence, the rod is adequate for static operation.

Fatigue Analysis

The fatigue loads experienced by the rod are identical to the manifold fatigue loads.

Stress Reduction Factors

For a smooth round tube, $K_t = 1$. The surface effect factor for the rod with a ground surface is $f_{su} = 1$. The reliability factor for steel is taken as .7. The size effect factor f_s is found to be .785, corresponding to a volumetric ratio of 42. The total stress reduction factor is therefore found to be $f_t = .55$. For 10^8 cycles, the allowable stress for 17-4PH steels is 60 ksi. From this, the allowable stress for the rod then can be evaluated and found to be $S_{en} = S \times f_t = 33$ ksi. The Goodman diagram for the rod is given in Figure 32.

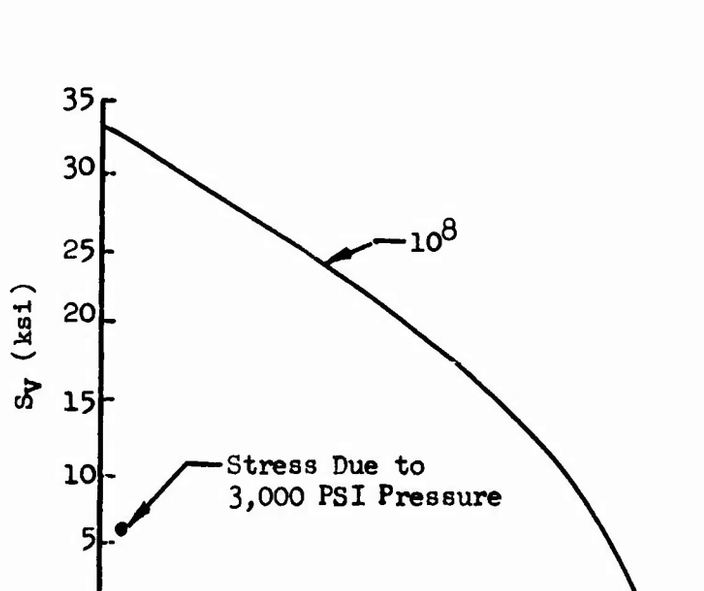

Figure 32. Goodman Diagram, Transfer Rod.

BYPASS VALVE CAP (PART NUMBER 38650-11022)

The bypass valve cap will be qualified by similarity to the cap currently in use on the CH-53 and CH-54 aircraft. These caps have been thoroughly substantiated in fatigue tests. The only difference between the caps is the thread type. A coarser thread was necessary to be compatible with the aluminum valve housing on the armored servo.

The following parts will also be accepted on the basis that they are currently operational parts:

65652-11228	Pressure Switch
65652-11206	Bypass Valve

LINKAGE ASSEMBLY (PART NUMBER 38650-11020)

The weakest part in the -11020 input linkage is the 11020-4 stem. The stem is machined from beryllium copper having a heat treat of 180,000 psi. The largest stress in the stem occurs in the undercut adjacent to the spherical bearing surface; see Figure 33.

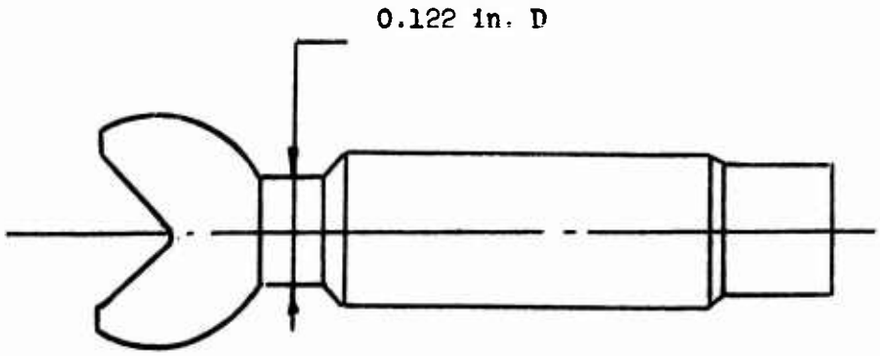

Figure 33. Linkage Assembly Dimensions.

The maximum load that can be applied to the valve stem is due to compression of the override spring and only occurs during a valve spool jam. This force F can be found from the expression

$$F = K \times X + F_p \qquad (29)$$

where K = spring constant of override spring, lb/in.

X = relative motion of inner and outer valve spool, in.

F_p = spring preload, lb

For a K of 114 lb/in. and a preload of 20 lb, the maximum load on the valve stem is 40 lb. The area in the undercut is equal to .0122 $in.^2$. The resulting stress is evaluated to be equal to 3,280 psi. A bending stress is superimposed on the basic tensile stress. This bending stress arises out of the nonlinearity of the rotary input and the friction of the spherical stem bearing and the housing. The force required to overcome the friction in the input arm was measured and found to be equal to 0.2 lb The section moment of inertia of the undercut is evaluated to be $I = 1.082 \times 10^{-5}$ $in.^4$; the resulting bending stress therefore is 1,130 psi. The total stress in the valve stem undercut is then found to be equal to 5410 psi. The margin of safety for the stem section is

$$MS = \frac{130,000}{1.15(5,410)} - 1 = +19.9, \text{ yield}$$

The flow forces (Bernoulli) acting on the valve spool may be evaluated from the expression

$$F = .0045 \times \text{Flow} \times \sqrt{\Delta P} \qquad (30)$$

At maximum flow rate, F = 3.12 lb. This force is less than the force experienced during override spring compression and is not additive.

INPUT LINK (PART NUMBER 38650-11017-1)

The input link is machined from 17-4PH stainless steel, heat treated to the H1025 condition.

The forces acting on the input link during normal flight operation are negligible. The loads that governed the design of the link are:

1. The dead weight of the swash plate and control system that must be reacted in the "power-off" mode.

2. Forces generated by the auxiliary servo and pilot input forces that must be reacted by the input link when the servo output is blocked.

Using the lateral mode, the force at the servo input corresponding to the pilot input force is found to be 1,290 lb. This loading exceeds the load due to the swash plate dead weight and will therefore be used in the analysis. The input link is represented in Figure 34. From geometry,

$\overline{AB}$ = 1.5 in.

$\overline{BC}$ = 1.125 in.

$|F_a|$ = 1290 lb

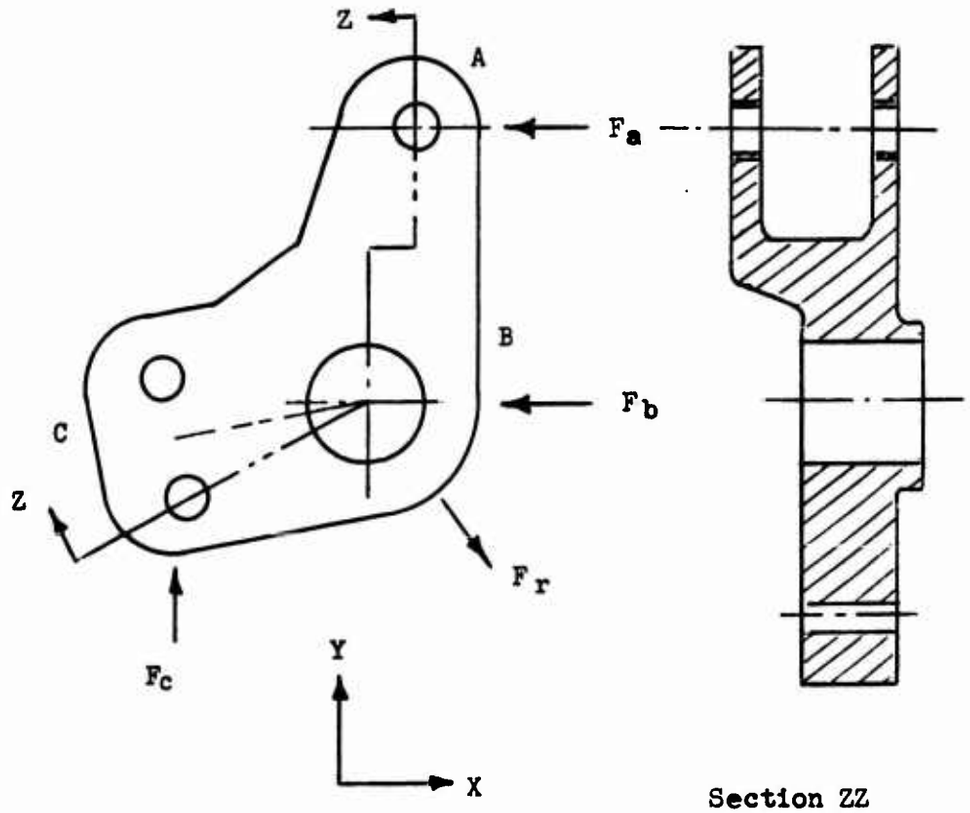

Figure 34. Input Link Dimensions.

The force F_c is evaluated to be F_c = 1,720 lb. The reaction force F_r which is transmitted to the input shaft is 2,140 lb. The force F_c must be reacted by the 38650-11017-7 pin and will be considered in the evaluation of the pin.

Lug Analysis of Input Clevis

Two separate stresses must be considered in the lug analysis: first, the stresses arising out of the external loading and second, the stresses due to the press fit of the NAS-537-4P-12 bushing into the lug. The stresses due to the press fit can be evaluated from the relationship

$$S = \frac{d}{b} \frac{(b^2 + c^2)}{\left[\frac{1}{E_2} \frac{b^2 + c^2}{c^2 - b^2} + u_1 + \frac{1}{E_1} \frac{a^2 + b^2}{b^2 - a^2} - u_2\right] (c^2 - b^2)} \qquad (31)$$

where

a = min ID of bushing, in.

b = max OD of bushing, in.

c/2 = min outside radius of lug, in.

d = max diametral interference, in.

S = max tensile stress in lug, psi

u_1 = Poisson's ratio for bushing material

u_2 = Poisson's ratio for lug material

E_1 = modulus of elasticity of bushing material, psi

E_2 = modulus of elasticity of lug material, psi

Substitution of values in the above relation yields

$$S = 11{,}700 \text{ psi}$$

The stress in the lug due to the external load is found using classical methods for transverse loaded lugs and is found to be equal to S = 21,050 psi.

The total stress in the lug is therefore found to be S_t = 32,750 psi, and the resulting margin of safety is

$$MS = 2.8 \quad \text{yield}$$

$$MS = 1.9 \quad \text{ultimate}$$

Therefore the input arm is considered adequate.

PIN (PART NUMBER 38650-11017-7)

The pin is machined from 17-4PH stainless steel, heat treated to the H1025 condition. The pin is loaded in shear with a force of 1,720 lb. See analysis of 11017-1 input arm.

The shear area of the bolt is .049 $in.^2$; the resulting stress is 35,000 psi and the corresponding margin of safety is

$$MS = 1.3 \quad \text{yield}$$

$$MS = .77 \quad \text{ultimate}$$

Therefore, the pin is found to be adequate.

INPUT SHAFT (PART NUMBER 38650-11017-2)

The shaft is machined from 17-4PH stainless steel, heat treated to the H1025 condition. From the analysis of the 11017-1 input link, it was found that the reaction force F_r that the link exerts on the shaft was 2,140 lb. This loading gives rise to both shear and bending stresses in the shaft. The maximum shear load occurs just outboard of the MKP-10A support bearing. The shaft shear area is .306 $in.^2$, and the resulting stress is 8,250 psi, which is well below the allowable of 93,000 psi.

The maximum bending stress occurs in the "O-ring" groove inboard of the outer support bearing. Bending is assumed possible inside the support bearing, since for small angular deflection the single-row bearing is assumed to offer no resistance to the bending moment.

By summing the forces about the input arm "O-ring" groove, we obtain the moment acting on that section. The numerical value for this moment is 2,110 in.-lb. The section moment of inertia, I, is .0308 $in.^4$, resulting in a bending stress of 15,250 psi, which is well below the static strength of the shaft.

SUPPORT BEARING MKP-10A

The Fafnir MKP-10A bearing is rated for a radial load of 6,700 lb, which is approximately three times the maximum applied load.

TUBING (PART NUMBER 38650-11014-4, -5)

The tubing material is 321 stainless steel having material properties of S_{tu} = 75,000 psi and S_{ty} = 30,000 psi.

The tubing is used to transfer fluid from the servo valve to the cylinder chambers and back. The tubes are furnace braced inside the second-stage piston. The tubing is subjected to both steady and vibratory pressures. These pressures will set up hoop stresses within the tubing. Axial loads are taken out in the end fittings. At proof pressure, the stress within the tubing is 20,500 psi; the margin of safety is

MS = +.27 yield

At P = burst pressure, the stress within the tubing increases to 34,100 psi. This is higher than the allowable yield; therefore, the tubing will yield under burst pressure loads, but will not rupture.

Fatigue Analysis

Assume a pressure fluctuation of ±500 psi about a mean pressure of 1,500 psi. This represents the maximum vibratory load derived from flight test data. The steady and vibratory stresses corresponding to these pressures are 6,670 ± 2,235 psi.

The maximum allowable endurance stress, S_{en}, for the tubing is 35,000 psi. The tubing is assumed to be in the "as-forged" condition. The total volume of the tubing is assumed to be stressed. With these assumptions, the stress reduction parameters are found to be

$f_{su} = .62$

$f_s = .702$

$f_r = .7$

$K_t = 2.5$ (concentration at fitting end)
$f_t = .305/K_f$

The allowable stresses as a function of frequency are given in Table XIII.

TABLE XIII. S_{en} AND N VALUES, TUBING

N	f_t	S_{en} (psi)
10^3	.229	8,030
10^4	.208	7,300
10^5	.18	6,320
10^6	.165	5,780
$10^{7,8}$	.157	5,500

The Goodman diagram for the tubing is shown in Figure 35.

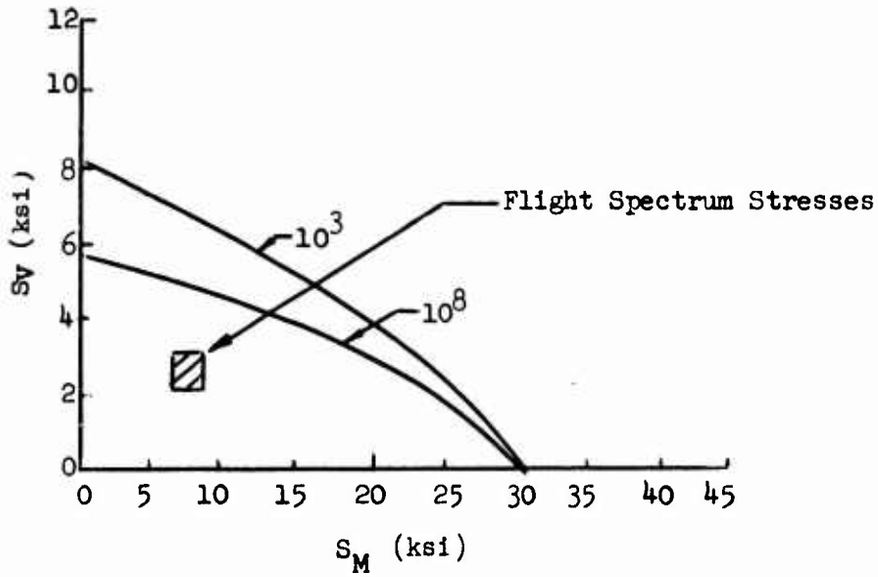

Figure 35. Goodman Diagram, Tubing.

From the Goodman diagram, it is evident that the tubing is good for vibratory flight load pressures.

TRUNNION (PART NUMBER 38650-11013-1)

The trunnion was machined from 4340 alloy steel, heat treated to 180,000 psi. The trunnion is part of the servo mounting and as such is subjected to the full servo output load or flight loads. Two criteria must be satisfied in the design of the trunnion. First, the trunnion must be structurally sound to carry all the imposed loads; second, the trunnion must be rigid enough to prevent positive feedback into the servo due to trunnion deflection.

Analysis

The trunnion is essentially a ring of nonuniform cross section. Loads are applied at two points on the ring and are reacted at two other points 90° removed. Because of the difficulty in analysis of this part, a computerized analysis was performed using a finite element and the ASKA program. A finite beam method and the FRAN program were also investigated but this was discarded in favor of the ASKA solution since FRAN does not account for all shear deflection.

The initial solutions showed that the trunnion was structurally adequate,

but was too soft to satisfy the stiffness criterion to prevent positive feedback. Accordingly, the trunnion cross section was increased to improve stiffness. The final configuration, which was fabricated, has a calculated stiffness of 1.82×10^6 lb/in. Since the stiffness criterion was determined to be more stringent, the trunnion is structurally adequate by a large margin.

SUPPORT BRACKET (PART NUMBER 38650-11023)

The bracket is machined from 4130 alloy steel sheet stock, heat treated to 180,000 psi. The support bracket provides the interface between the servo and the aircraft. The shape and dimensions of the bracket were dictated by the existing aircraft configuration. For subsequent designs, providing a suitable mounting point on the aircraft transmission will eliminate the need for the bracket. The bracket is subjected to the same loading as the trunnion.

Static Analysis

The bracket dimensions are shown in Figure 36. Assume that only the side webs react any bending. Now let

F_1 = load force, lb

F_x = horizontal component of F_1, lb

F_y = vertical component of F_1, lb

M_1 = reaction moment at A, in.-lb

M_2 = reaction moment at B, in.-lb

R_A = vertical reaction force at C, lb

R_B = horizontal reaction force at C, lb

Θ = angle between the load and vertical axis of the bracket

The load F_1 can vary from +F to -F, depending on which direction the servo loads act. F_1 is positive, as shown in Figure 36, and let Θ be equal to the maximum misalignment due to swash-plate rotation.

1. Section I

   Assume that point A cannot react any vertical forces. Thus, all vertical loads are taken out by the moment M_1. Referring to Figure 36 sections were taken through critical areas. These are indicated in Figure 36 and numbered 1 through 5. By evaluating the moments of inertia and the cg location of each section of the complete U-shaped bracket, we may evaluate the stresses at each section as a function of the load, the section area, cg location and section moment of inertia. For Section I, the

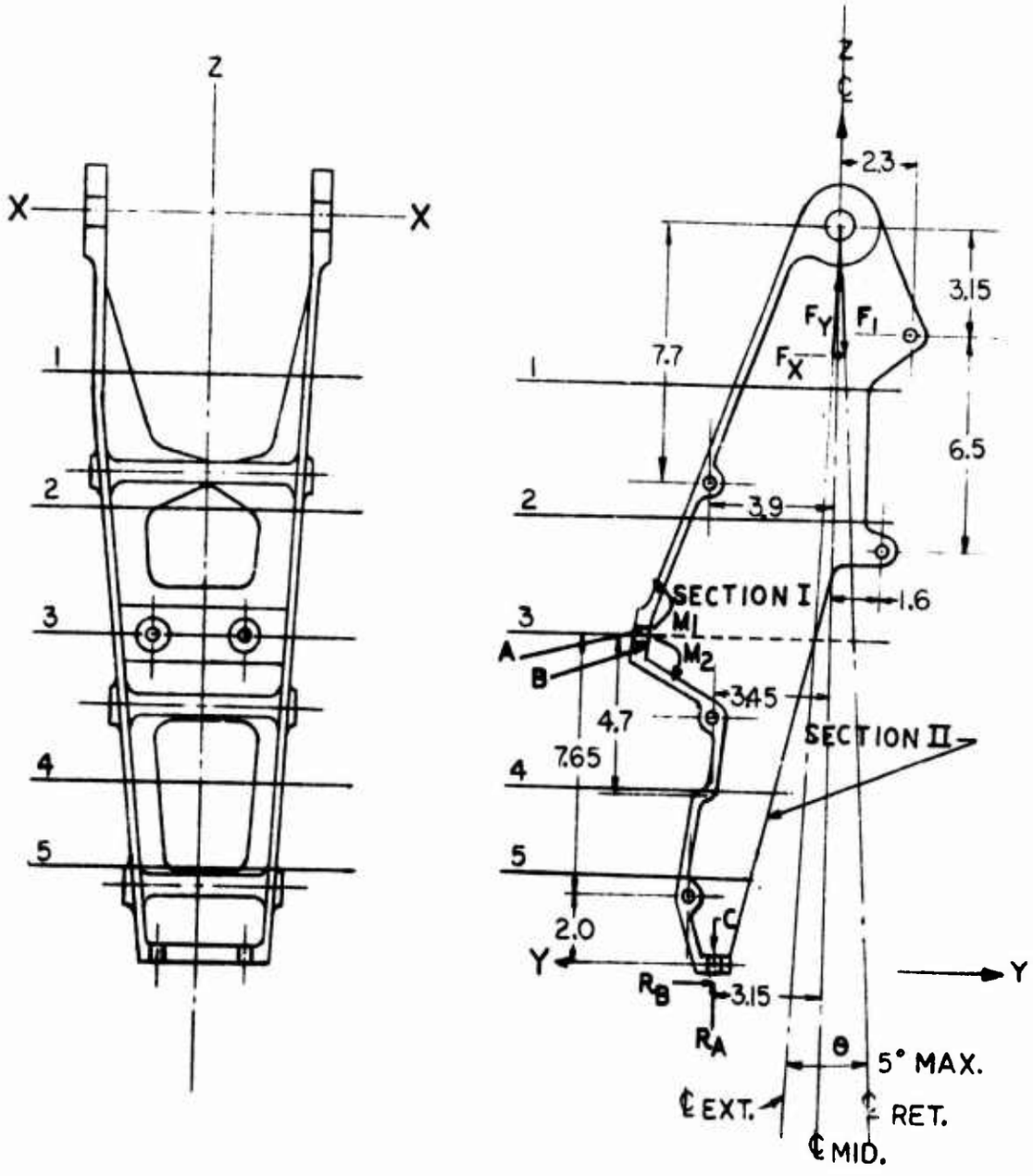

Figure 36. Support Bracket.

moments of inertia for Sections 1, 2 and 3 are

$I_1 = 7.553$ in.^{4}

$I_2 = 11.002$ in.^{4}

$I_3 = 14.34$ in.^{4}

The resulting static stresses are

$S_1 = 21{,}900$ psi

$S_2 = 27{,}080$ psi

$S_3 = 31{,}600$ psi

where S is found from the relation

$$S = F/A + M_c/I \tag{32}$$

where F = applied load, lb

A = section area, in.^{2}

M = bending moment, in.-lb

C = distance to point of interest, in.

I = section moment of inertia, in.^{4}

S = stress, psi

2. Section II

The end moment M_2 in Section II can be replaced by a force F acting on the centroid of the section. This is possible since the axis of the subsection centroids is a straight line for Section II.

The two reaction forces R_A and R_B can thus be found.

$$F = M_2/r$$

$$R_A = -F$$

$$R_B = M_2/h$$

where r = distance from point B to centroidal axis

h = height of Section II

The moments of inertia of Sections 4 and 5 are

$I_4 = .5123$

$I_5 = .4920$

The resulting stresses are

$S_4 = 30{,}500$ psi

$S_5 = 31{,}600$ psi

and the reaction forces are

$R_A = 21{,}100$ lb

$R_B = 14{,}500$ lb

The forces R_A and R_B must be reacted by the two 1/2-in.-diameter mounting bolts in shear and tension. The maximum allowable loads for the bolts are 24,000 lb tension and 18,650 lb shear for each bolt.

For each bolt, the tensile load is $R_A/2 = 10{,}550$ lb and the shear load is $R_B/2 = 7{,}250$ lb. Hence, the bolts are adequate.

The maximum stress occurs in Section 5 of the bracket. The magnitude of the stress is 31,600 psi. The margin of safety is

$MS = 3$ yield

$MS = 2.06$ ultimate

Statically, the bracket is adequate.

Fatigue Analysis

Assume that the loads are reacted through the side plate, and the center plate only prevents buckling of the sides. For the flat plate, we assume $K_t = 1$. This is permitted, since the major load path does not pass through any stress risers. The following stress reduction factors were evaluated for the bracket:

$f_{su} = .464$

$f_s = .7$

$f_r = .7$

$f_t = .227$

For the two maximum flight loads, the maximum stress at Section 5 becomes

$$S_1 = 2{,}610 \pm 6{,}750 \text{ psi}$$

$$S_2 = 10{,}150 \pm 4{,}250 \text{ psi}$$

The Goodman diagram is shown in Figure 37.

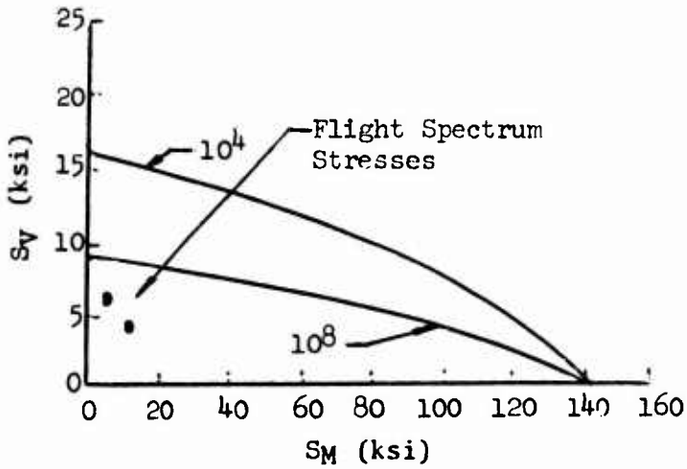

Figure 37. Goodman Diagram, Support Bracket.

From the Goodman diagram, it can be seen that the bracket is adequate in fatigue for the load spectrum imposed on it.

Bracket Deformation

The bracket will deform under load both in shear and bending. To simplify the solution, we assume that the shear deflection occurs only on an axis coinciding with the line of loading. The shear area along this line is 8.28 in.^{2}. The shear deformation may be evaluated from the following:

$$d_s = \frac{FL}{AG} \tag{33}$$

where d_s = shear deflection, in.

F = applied force, lb

L = length of shear path, in.

A = area of shear section, $in.^2$

G = shear modulus, psi

Substitution of values yields

$d_s = 5.84 \times 10^{-4}$ in. for an applied force of 21,200 lb

The deflection due to bending can be found from

$$d_b = \frac{FL^3}{3EI} \tag{34}$$

where d_b = deflection, in.

F = applied force, lb

L = length of beam, in.

E = modulus of elasticity, psi

I = moment of inertia, $in.^4$

To facilitate use of this formula, we treat the bracket like a short cantilever beam. Substitution of numerical values into the above expression for an applied force of 21,200 lb results in a deflection of

$$d_b = 2.73 \times 10^{-3} \text{ in.}$$

The total deflection then is

$$d = d_s + d_b \tag{35}$$

$$d = 3.314 \times 10^{-3} \tag{36}$$

The total stiffness of the bracket then is

$$K = \frac{F}{d}$$

$$K = 6.43 \times 10^6 \text{ lb/in.}$$

The total stiffness of the servo support is the series combination of the trunnion and support bracket spring rates. For springs in series, we have

$$K = \frac{(K_1 K_2)}{(K_1 + K_2)} \tag{37}$$

Substitution of values into the above relationship yields

$$K_t = 1.42 \times 10^6 \text{ lb/in.}$$

This is the value for the support spring that must be used in the stability analysis.

APPENDIX II
SERVO ANALYSIS

SERVO POWER REQUIREMENT

Two power requirements are of interest:

1. Maximum power to assure pump adequacy.

2. Standby power to assure proper cooling flow.

MAXIMUM POWER REQUIRED

The maximum power requirement is dictated by a 100-percent-per-second control stick input in either mode. The maximum servo displacement occurs in the collective mode and is equal to 2.703 in. The flow corresponding to this rate is

$$Q = X_p A_p = 2.703 \times 3.54 = 9.56 \text{ in.}^3/\text{sec}$$

Expressed in gallons per minute,

$$Q = 2.49 \text{ gpm/stage/servo}$$

The horsepower required per stage per servo at 3000 psi supply pressure is

$$hp = \frac{3000 \times 2.49}{1740} = 4.28$$

Total flow required per stage for three servos is 7.47 gpm (max).

The pump capacities at sea level and standard day for the CH-54B aircraft are 11.1 and 15.1 gpm for the first and second stages, respectively. Therefore, the pumps are adequate to fulfill the maximum flow requirement.

STANDBY POWER REQUIREMENT

The cooling flow restrictor used in the existing servo in the second stage has been retained in the integral armored servo. The first-stage system does not require a cooling flow restrictor in the primary servo circuit. In this stage the cooling flow is provided by a separate system.

The servo leakage at null is equal to that of the 6465-62161 servo, since the armored servo and the 6465-62161 servo use the same basic valve spool and sleeve. The null leakage is approximately .12 gpm per valve at a fluid temperature of 165°F. Since the null leakage rate is the same for both model servos, it is concluded that sufficient cooling flow will be provided by the integral armored servo.

SERVO VALVE FLOW GAIN

The flow gain of the valve is defined as

$$K_V = \left.\frac{\partial Q}{\partial X_v}\right|_{P = \text{constant}} \tag{38}$$

This can be rewritten as

$$K_V = \frac{\partial (C_D A_o \sqrt{(2g/d)\ P})}{\partial X_v} \tag{39}$$

In general, this is a nonlinear expression. However, the use of a square-holed orifice linearizes the flow gain. Neglecting saturation effects, the flow gain of a square holed orifice can be represented by a constant. Its value is found from an expression which is independent of the valve opening :

$$K_V = C_d \cdot w \cdot \sqrt{(2g/d)\ P} \tag{40}$$

Substituting numerical values,

$$K_V = .635 \times .074 \times \sqrt{(2 \times 386/.0309) \times 3{,}000}$$

$$K_V = 287.66 \text{ in.}^2/\text{secsq}$$

SERVO TIME CONSTANT

The servo time constant is defined as

$$t = \frac{A_p}{K_V} \text{ sec} \tag{41}$$

This is valid for all inputs except those in the region of valve saturation.

Substitution of numerical values into equation 41 yields the time constant for the integral armored servo:

$$t = \frac{3.54}{287.66} = .0123 \text{ sec}$$

The break frequency of the servo is defined as the reciprocal of the time constant. Thus, the frequency is

$$W_B = \frac{1}{t} \tag{42}$$

$$W_B = 8.4 \text{ rad /sec}$$

This equates to a frequency of 12.95 cycles per second.

The break frequency is a measure of the response range of the servo. Beyond W_B the response of the servo will diminish by 20 db/decade. The value of W_B of the servo is high enough to respond to all pilot and autopilot inputs and low enough to attenuate the high-frequency modes of the external load.

SERVO VALVE PRESSURE GAIN

The pressure gain K_p is defined as

$$K_p = \left.\frac{\partial P}{\partial X_v}\right| \quad X_p = \text{constant} \tag{43}$$

For a square-holed orifice, this gain is a constant except in the saturation and underlap region and is equal to the slope of the pressure vs. valve displacement curve. This curve is shown on Figure 46.

The numerical value of $K_p = \frac{2050 \text{ psi}}{.00072 \text{ in.}} = 2.85 \times 10^6 \frac{\text{psi}}{\text{in.}}$

at $X_v = 0$

BLADE IMPEDANCE

The blade impedance was evaluated from ground test data and blade characteristics. Ground testing established a value for the natural frequency of the rotating system. The equivalent mass of the blade was calculated using a multiple mass beam analysis, using known masses and deflections along the blade.

STABILITY ANALYSIS

The stability of a servo is greatly affected by the characteristic of the external load. For the helicopter, the servo load system can be represented by the mathematical model shown in Figure 38,

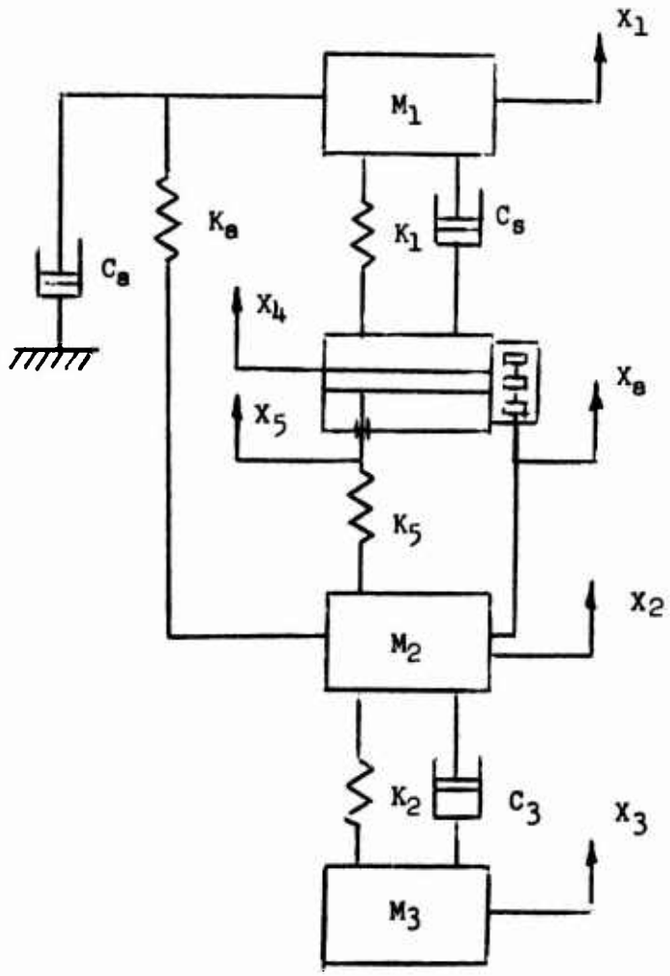

Figure 38. Servo Valve Gain.

where M_1 = equivalent blade mass, lb-sec^2/in.

M_2 = equivalent pylon mass, lb-sec^2/in.

M_3 = equivalent fuselage mass, lb-sec^2/in.

K_1 = combined swash plate and torsional blade stiffness, lb/in.

K_2 = equivalent fuselage stiffness, lb/in.

K_a = aerodynamic stiffness acting on the fuselage due to a pitch input, lb/in.

C_3 = fuselage structural damping, lb-sec/in.

C_a = aerodynamic blade damping, lb-sec/in.

Before the equations of motion can be written for the system of Figure 38, it is necessary to develop the servo equation. Refer to Figure 39.

From the equation of continuity and neglecting any compressibility effects, we can write for an equal area actuator,

Flow Into Servo = Flow Out of Servo

or

$$Q_{in} = Q_{out} \tag{44}$$

where Q = flow in, cu in./sec

The equation of flow through a square-holed orifice is

$$Q = C_d \, W \cdot X_v \sqrt{(2g/d)P} \tag{45}$$

where C_d = orifice coefficient

W = width of orifice, in.

X_v = valve opening, in.

g = gravitational constant, in./sec^2

d = fluid density lb/cu in.

P = pressure gradient across the orifice, psi

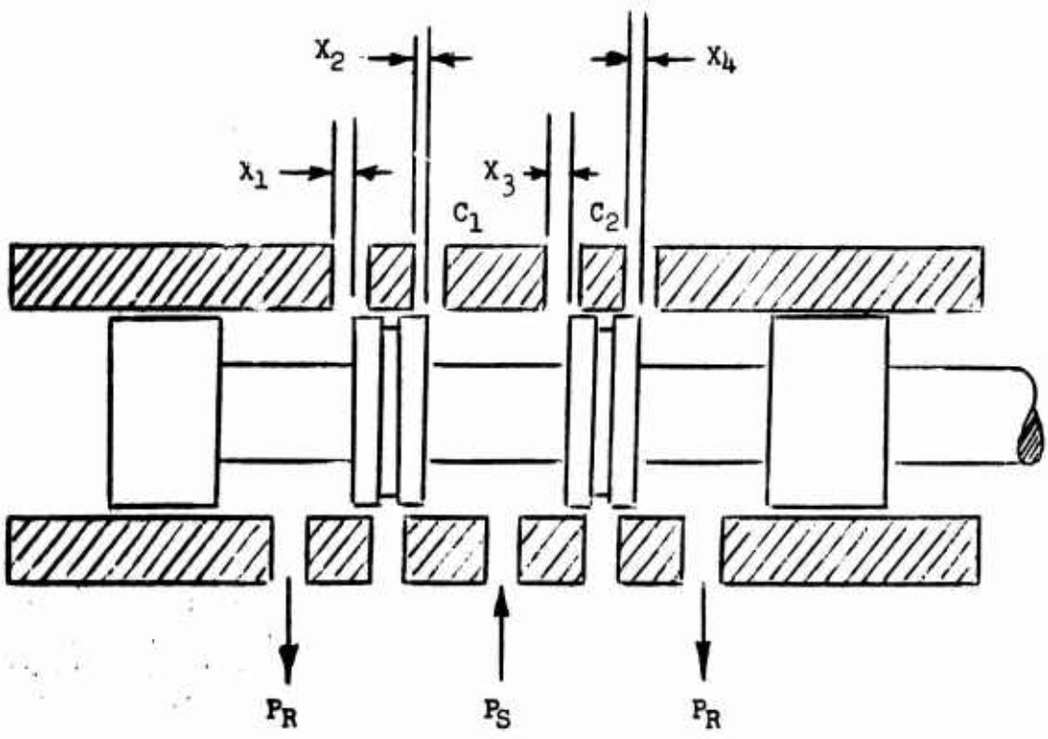

Figure 39. Servo Valve.

We define the hydraulic conductance k as

$$k = C_d W \sqrt{2g/d} \tag{46}$$

Equation 44 can now be rewritten as

$$k\left[(X_1 + X_v)\sqrt{P_s - P_{c1}} - (X_2 - X_v)\sqrt{P_{c1} - P_r}\right]$$
$$= k\left[(X_3 - X_v)\sqrt{P_s - P_{c2}} - (X_4 - X_v)\sqrt{P_{c2} - P_r}\right] \tag{47}$$

where X_1, X_2, X_3, X_4 = valve underlap, in.

P_s = supply pressure, psi

P_r = return pressure, psi

P_{c_1} = chamber 1 pressure, psi

P_{c_2} = chamber 2 pressure, psi

For a nonpressurized reservoir, as used on the CH-54 aircraft, P may be taken as zero. From stability considerations, we are interested in the rate of change of flow into or out of the servo either due to an external input or due to variations in the servo load. It is known that the rate of change of flow in the servo is dependent on the change in valve opening as well as the change in the pressure across the orifice. Mathematically this can be expressed as

$$dQ = \frac{\partial Q}{\partial X_v}\Bigg|_{P = \text{Constant}} dX_v + \frac{\partial Q}{\partial P}\Bigg|_{X_v = \text{Constant}} dP \tag{48}$$

Differentiating Equation 47 with respect to valve opening and pressure,

$$\left[k\ (P_s - P_{c1}) + k\ P_{c1}\right]dX_v - \left[(k\ (X_1 + X_v)/2)\ (P_s - P_{c1})^{-1/2}\right.$$
$$\left. + (k\ (X_2 - X_v)/2)(P_{c_1})^{-1/2}\right]dP + \left[k\sqrt{P_s - P_{c_2}} + k\sqrt{P_c}\right]dX_v$$
$$- \left[(k(X_3 + X_v)/2)\ (P_s - P_{c_2})^{-1/2} + (k\ (X_4 - X_v)/2\ (P_{c_2})^{-1/2}\right]dP = 0 \tag{49}$$

Equation (49) can be expressed in a simplified form as

$$(K_1 + K_3)dX_v - (K_2 + K_4)dP = 0$$

C_v and C_p are defined as

$$C_v = (K_1 + K_3) \tag{50}$$

$$C_p = -(K_2 + K_4) \tag{51}$$

With this definition we can write equation (48) as

$$dQ = C_v\, dX_v + C_p\, dP \tag{52}$$

The quantity dQ is the total change in flow past the servo valve. The quantities C_v and C_p are the partial derivatives of Q with respect to X_v and P respectively. For small disturbances about a quiescent operating point, the two partial derivatives are nearly linear and may be taken as constants, evaluated at that operating point.

The total orifice flow is divided into several flows, such that the change in flow is

$$dQ_T = Q_D + Q_H + Q_A \tag{53}$$

where Q_T = total flow, cu in./sec

Q_D = damping flow, cu in./sec

Q_H = compressibility flow, cu in./sec

Q_A = actuator flow, cu in./sec

From the definition of the bulk modulus B,

$$B = (\Delta P_o)/\Delta V/V \tag{54}$$

where B = bulk modulus of the fluid, psi

ΔP_o = incremental change in load pressure, psi

ΔV = incremental change in volume, cu in.

V = total volume under compression, cu in.

During normal flight operations the helicopter main rotor servos are approximately at midstroke; therefore the upper chamber volume V_1 is very nearly equal to the lower chamber volume V_2. Hence, we can say $V_1 = V_2 = V/2$. Consequently,

$$\Delta V_1 = \Delta V_2 = \Delta V/2 \tag{55}$$

The change in load pressure, P, can be expressed in terms of P_o, such that

$$\Delta P = 2\Delta P_o \tag{56}$$

Substitution of equations (55) and (56) into (54) yields

$$\Delta P = 4B\Delta V/V \tag{57}$$

Differentiating equation (55) with respect to true yields

$$\Delta P/\Delta t = (4B/V)(\Delta V/\Delta t) \tag{58}$$

In the limit, as Δt approaches zero, equation (56) becomes

$$dp/dt = (4B/V)dV/dt \tag{59}$$

The compressibility flow Q_H is expressed as

$$Q_H = dV/dt \tag{60}$$

Substitution of equation (60) into equation (59) yields the desired relationship of Q_H:

$$Q_H = (V/4B)dP/dt \tag{61}$$

The actuator flow, Q_A, is the integrating flow of the servo, which expressed mathematically is

$$Q_A = Adx/dt \tag{62}$$

where d_x/d_t = differential of the pistcn displacement with respect to time, in./sec.

The damping flow, Q_D, is made up of the leakage across the piston head seal and the leakage across the servo valve lands. The piston head seal leakage in this servo is very much smaller than the valve leakage and may be neglected. Then Q_D becomes

$$Q_D = C_D\Delta P \tag{63}$$

The leakage coefficient C_D can be evaluated from the relationship of flow between two flat plates. Assuming the plates as bend to form a circle, we may express the flow Q as

$$Q = (Kd^3\pi D)(1 + 1.5e)(\Delta P)/(uL) \tag{64}$$

where
- D = diameter of valve spool, in.
- d = diametrical clearance between spool and sleeve, in.
- μ = viscosity of fluid, centipoise, dyne-sec/cm^2
- L = length of flow path, in.
- e = eccentricity
- P = pressure gradient across path, psi
- K = constant of proportionality

From equation (64) the leakage coefficient becomes immediately evident:

$$C_D = Kd^3 \pi D(1 + 1.5e)/(\mu L) \tag{65}$$

Substitution of numerical values into equation (65) yields a value for $C_D = 1 \times 10^{-5}$ in.^{5}/lb-sec.

Substitution of equations (59),(60) and (61) into equation (51) yields

$$dQ_T = C_D dP + (V/4B)dP/dt + Adx/dt \tag{66}$$

Equating equations (50) and (66) results in the final servo equation:

$$C_v dX_v + C_p dP = C_D dP + (V/4B)\, dP/dt + Adx/dt \tag{67}$$

From Figure 38, $dX_v = X_2 - X_4$, and $dX = X_4 - X_5$. The equations of motion for the system of Figure 38 can now be written as follows:

$$M_1\ddot{X}_1 + C_A \dot{X}_1 + K_1 (X_1 - X_4) = 0 \tag{68}$$

$$M_2\ddot{X}_2 + C_3(\dot{X}_2 - \dot{X}_3) + K_2(X_2 - X_3) + K_5(X_2 - X_5) = K_A X_1 \tag{69}$$

$$M_3\ddot{X}_3 + C_3(\dot{X}_3 - \dot{X}_2) + K_2 (X_3 - X_2) = 0 \tag{70}$$

$$K_1(X_4 - X_1) + K_5(X_5 - X_2) = 0 \tag{71}$$

$$C_v X_a + C_p dP = C_d \Delta P + V/(4B)\dot{dP} + A(\dot{X}_4 - \dot{X}_5) \tag{72}$$

$$C_2 = V/4B \tag{73}$$

$$X_a = X_2 - X_4 + a(X_3 - X_2) \tag{74}$$

$$dPA = K_1(X_4 - X_1) \tag{75}$$

$$C_1 = C_p + C_D \tag{76}$$

Elimination of several variables and transformation yields the final system matrix:

$$
\begin{bmatrix}
K_1+C_AS+M_1S^2 & 0 & 0 & -K_1 & 0 \\
-K_4 & K_5+K_2+C_3S+M_2S^2 & -K_2+C_3S & 0 & -K_5 \\
0 & -K_2+C_3S & K_2+C_3S+M_3S^2 & 0 & 0 \\
(C_1+C_2S)K_1 & C_vA(1-a) & C_vA_a & -(K_1C_1+C_vA)+(K_1C_2+A^2)S & A^2S \\
-K_1 & -K_5 & 0 & K_1 & K_5
\end{bmatrix}
\begin{bmatrix} X_1 \\ X_2 \\ X_3 \\ X_4 \\ X_5 \end{bmatrix} = 0
$$

The characteristic equation can be evaluated from the determinant of the matrix. From the roots of the characteristic equation, the system stability can be determined.

The aircraft parameters used in the evaluation are listed below in Table XIV. All values are referred to the servo.

TABLE XIV. PARAMETRIC VALUES

Parameter	Value	Units
M_1	2.16	lb-sec^2/in.
M_2	38.9	lb-sec^2/in.
M_3	31.1	lb-sec^2/in.
K_1	29500	lb/in.
K_2	62500	lb/in.
K_5	1.6×10^6	lb/in.
K_A	0	lb/in.
C_1	.00201	in.^{5}/lb-sec
C_2	.000019	in.^{5}/lb-sec
C_3	465	lb-sec/in.
C_A	10.	lb-sec/in.
C_V	280	in.^{2}/sec
A	3.52	in.^{2}
a	0	

The solution of the system matrix for the values given in Table XIV was obtained using the UNIVAC 1108 computer. The roots of the system are given in Table XV. For the analysis, the swash-plate damping C_S was assumed to be zero.

TABLE XV. SYSTEM ROOTS	
Real Part	Imaginary Part
-12.929	± S 57.83
-.432	± S 116.82
-.0232	± S 3.435
-79.28	

Since the real parts of all roots are negative for this servo actuator, the system is stable.

APPENDIX III

TEST REPORT

ENGINEERING TEST PLAN FOR INTEGRAL ARMORED SERVO

The following tests are proposed to meet the requirements of Contract No. DAAJ02-70-C-0051, paragraphs 2.d(1) through 2.d(3):

1.0 TEST CONDITIONS

1. Ambient Temperature 70° ± 20°F

2. Fluid Temperature 80° ± 20°F

3. System Filtration 5 micron nominal, 15 absolute (per MIL-F-8815)

4. Fluid MIL-H-5606A

5. Normal Operating Supply Pressure First Stage 3,000 psi
   Second Stage 3,000 psi

6. Normal Operating Return Pressure 30 psi

7. Flow Required 4 gpm First Stage
   4.5 gpm Second Stage

2.0 PRIOR TO ASSEMBLY OF THE SERVO:

The servo valve will be mounted in a ported test block to obtain the following information:

1. Servo Valve Pressure Gain Characteristics

   Valve spool displacement will be measured with a dial indicator and cylinder port pressure monitored with a direct reading pressure gauge. All data will be recorded on test record sheets. A plot of pressure versus spool displacement will be made.

2. Servo Valve Flow Gain Characteristics

   Valve spool displacement will be measured with a dial indicator, and cylinder port flow will be monitored using a graduated cylinder and stop watch to provide flow versus spool displacement data. All data will be recorded on test record sheets.

3. Servo Valve Force

   The force required to displace the spool of the servo valve through full displacement at zero and at full operating pressure

will be measured using a spring scale. Test data will be recorded on test record sheets.

3.0 AFTER ASSEMBLY OF THE SERVO

1. Proof Pressure

Both stages of the servo shall be proof tested. The servo shall be pressurized to 4,500 psi on either stage, the alternate stage being vented to atmosphere for a 2-minute period at full extend and at full retract. This proof pressure procedure shall be repeated for a second time. The servo shall be cycled before, between and after the two tests. At the completion of this test, the other stage shall be proof tested in a similar manner. During each proof pressure application there shall be no evidence of leakage at any joint or boss and no loosening or permanent deformation of the unit. Any abnormalities shall be recorded on the test record sheets.

2. Internal Leakage

Leakage shall be measured from each stage at normal operating pressure with the power piston stationary and off the stops. Leakage shall be between 500 cc/min and 1,650 cc/min for each stage and shall be measured at the applicable return port using graduated cylinder and stop watch. Similar measurements shall be made with power piston bottomed and the servo input bottomed in the sloppy link. Leakage shall be between 16 cc/min and 30 cc/min for each stage. All measurements shall be recorded on the test record sheets.

3. External Leakage

The servo shall be cycled through full stroke at normal operating pressure for a minimum of 25 full stroke cycles. If any external leakage is apparent, sufficient additional cycling shall be performed to determine that the leakage does not exceed one drop in 25 full stroke cycles. All measurements shall be recorded on the test record sheets.

4. Input Force

The force required at the servo input shall be measured with each stage individually on at normal operating pressure and shall not exceed 2 pounds. A similar measurement made with both stages of the servo on shall not exceed 4 pounds. The force shall be measured using a graduated spring scale. All measurements shall be recorded on the test record sheets.

5. Input Linkage Spring Rate

The spring rate of the servo input linkage shall be determined by rigidly fixing one end of the linkage and measuring deflection versus load at the free end. Load shall be applied through a force gage and deflection measured with a dial indicator. All results shall be recorded on the test record sheets.

6. Response Characteristics

The response characteristics of the servo will be determined by driving the servo with an H53 AFCS servo and servo analyzer, at operating pressure and no load, from zero to approximately 20 cps. Response characteristics $\frac{\text{Output Disp.}}{\text{Input Disp.}}$ versus frequency will be plotted.

7. Actuator Stroke

With normal operating pressure applied to both stages, the servo shall be operated through full stroke and the stroke of the power piston measured using a dial indicator. The stroke shall be between 5.680 and 5.590 inches. This measurement shall be recorded on the test record sheets.

4.0 TEST LOG

A log of tests to be accomplished and tests completed shall be maintained. Calibration dates will be recorded of all test equipment and all instrumentation used.

5.0 MOTION PICTURES

In accordance with DD 1423 data Item 01-009 of the subject contract, a motion picture film record of the test program will be taken.

TEST DATA

The hydraulic test panel used during the bench tests of the valve and servo assembly is shown on Figure 40. Figures 41 and 42 illustrate the servo test installation and the frequency response test equipment, respectively. The servo valve flow gain and pressure gain test data are summarized in Tables XVI and XVII, respectively. Figure 45 shows the plots of the flow gain test data of the armored servo valve and a CH-54B production valve.

Plots of the valve pressure gain are shown in Figure 46 for the armored servo valve and the CH-54B valve. From these plots it can be seen that the performance of the armored servo valve is identical to the production CH-54B valve. This was expected, since both servos share the same valve.

The servo no-load frequency response test data of the armored servo are summarized in Table XVIII, plots of this data are shown on Figures 43 and 44. Test data of a CH-54B servo is added to Figure 43 for comparison.

From the plots it can be seen that the performance of the armored servo is equal to that of the standard production servo. This is no coincidence since the gains and other pertinent performance parameters were made identical by design.

Figure 40. Hydraulic Test Panel.

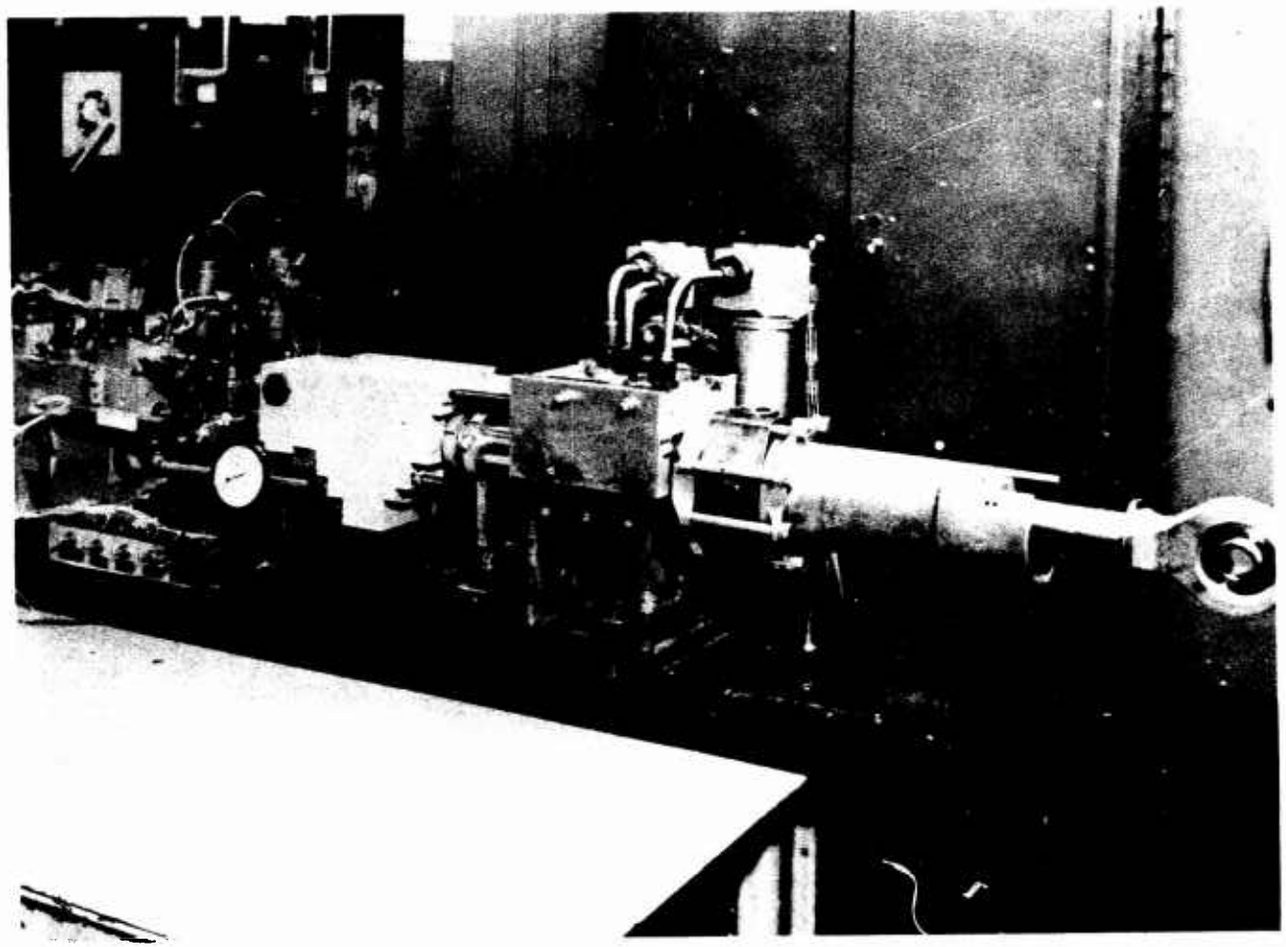

Figure 41. Servo Test Assembly.

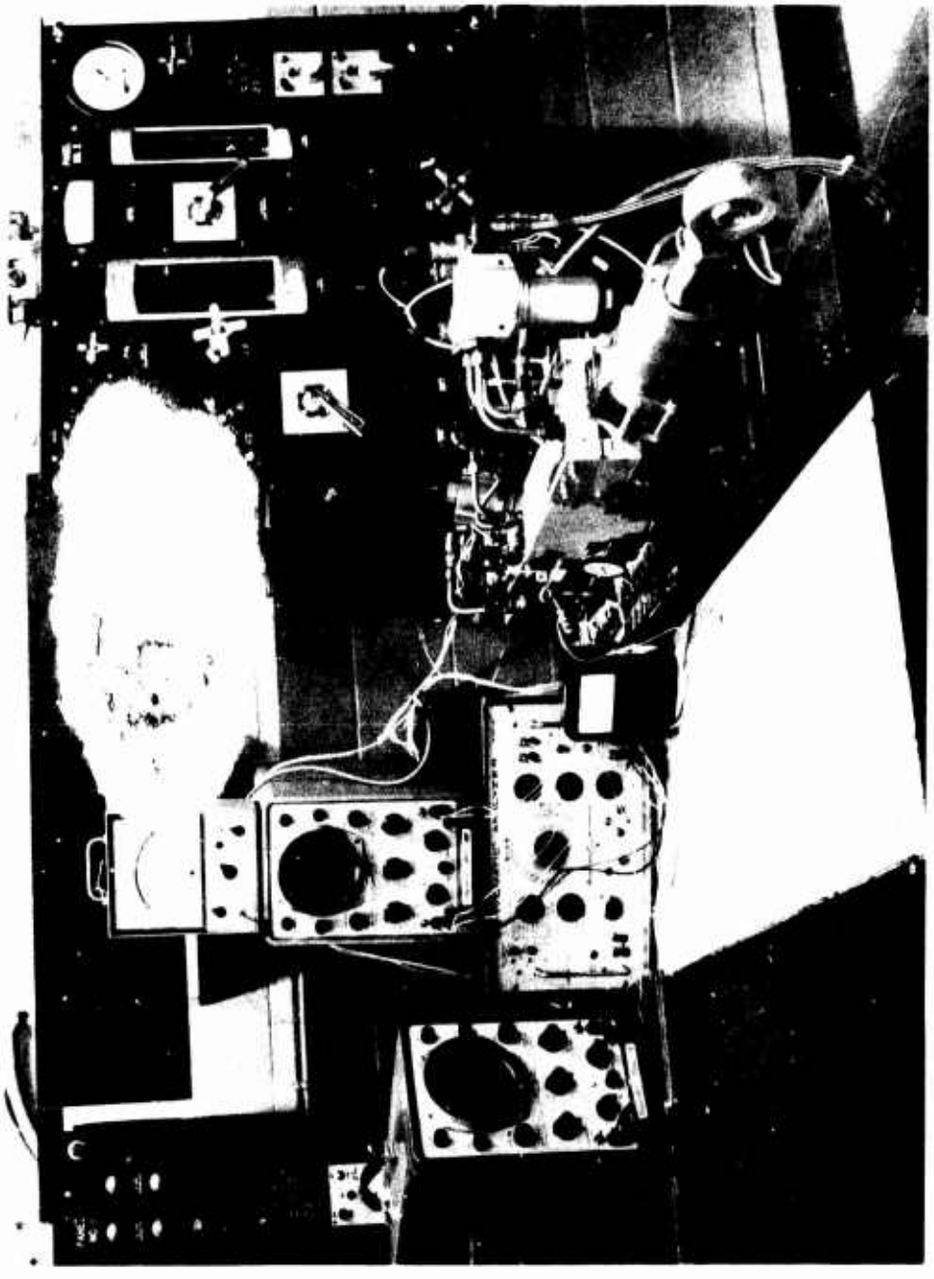

Figure 42. Frequency Response Test Setup.

TABLE XVI. SERVO VALVE FLOW GAIN CHARACTERISTICS				
Displacement (in.)	Q_1 (gpm)	Q_2 (gpm)	Oil Temp (°F)	P (psi)
0	.17	-	100	3000
.010	1.8	-	110	3000
.020	2.2	-	112	2980
.030	3.2	-	114	2950
.040	4.05	-	116	2920
.050	5.0	-	118	2900
.060	5.92	-	119	2900
.070	6.65	-	119	2880
.080	6.85	-	121	2870
.090	7.4	-	123	2740
.100	7.8	-	123	2080
0	-	.15	121	2960
-.010	-	1.14	122	2940
-.020	-	2.4	123	2910
- 030	-	3.25	125	2880
-.040	-	4.2	125	2860
-.050	-	5.15	125	2840
-.060	-	6.05	126	2830
-.070	-	6.68	126	2800
-.080	-	6.75	128	2800
-.090	-	7.2	129	2660
-.100	-	7.8	130	1990

TABLE XVII. SERVO VALVE PRESSURE GAIN CHARACTERISTICS

Displacement x 10^{-4} (in.)	P_{c_1} (psi)	P_{c_2} (psi)	T_{oil} (°F)	P (psi)
0	1480	1480	122	2980
2	1730	1300		
4	1960	1010		
6	2190	810		
8	2370	560		
10	2520	510	121	2980
12	2660	400		
14	2740	310		
16	2800	250		
18	2850	190		
20	2880	160		
22	2900	140		
25	2920	110		
30	2940	90	119	2980
40	2960	70		
50	2980	50		
60	2980	40		
70	2980	30		
80	2980	30		
90	2990	25		
100	2990	25	117	

TABLE XVIII. SERVO RESPONSE CHARACTERISTICS				
Freq. (Hz)	X_{In}	X_{Out}	Total Phase Lag (deg)	Driver Phase Lag (deg)
1	6.8	6.8	-	43
3		6.8	84	80
5		6.6	117	107
7		6.4	137	113
9		6.0	154	121
11		5.2	166	123
13		4.6	190	125
15		4.3	196	130
17		4.0	212	135
19		3.9	224	137
2:	6.8	3.1	242	141

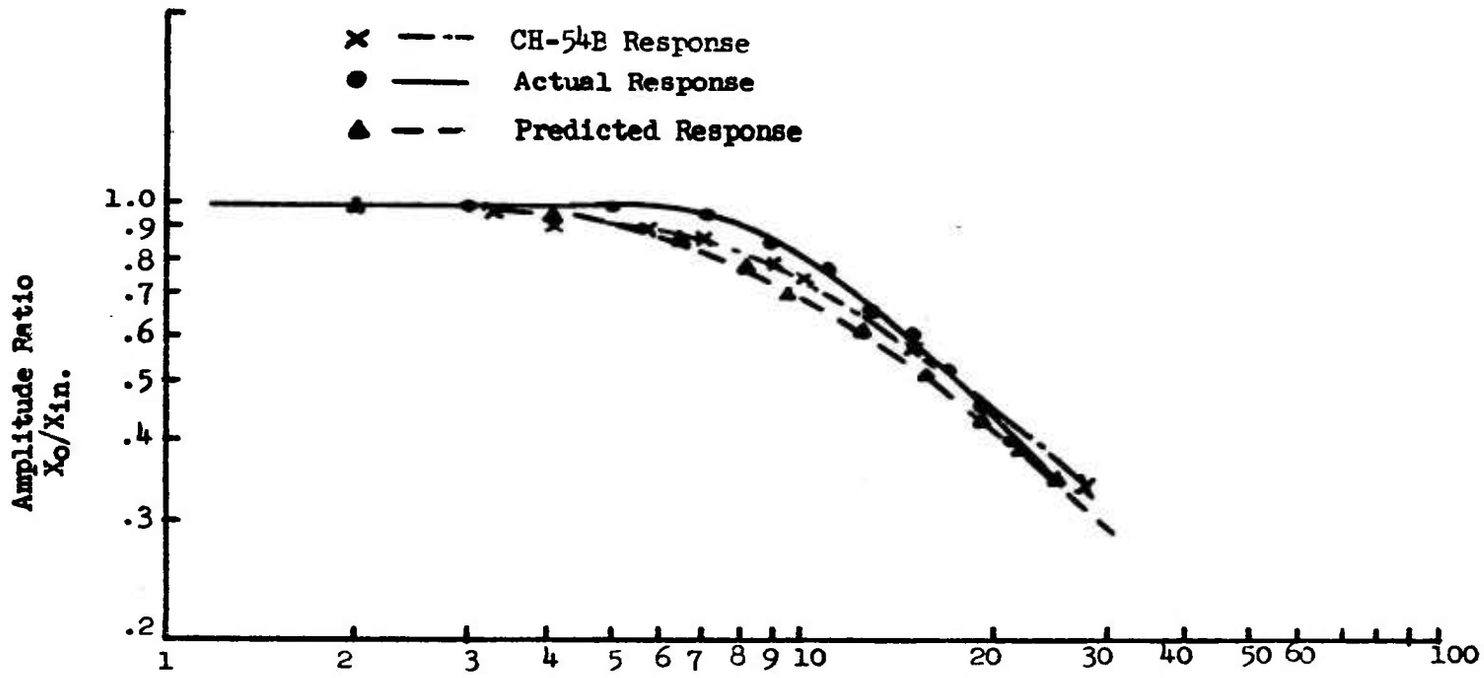

Figure 43. Armored Servo Frequency Response.

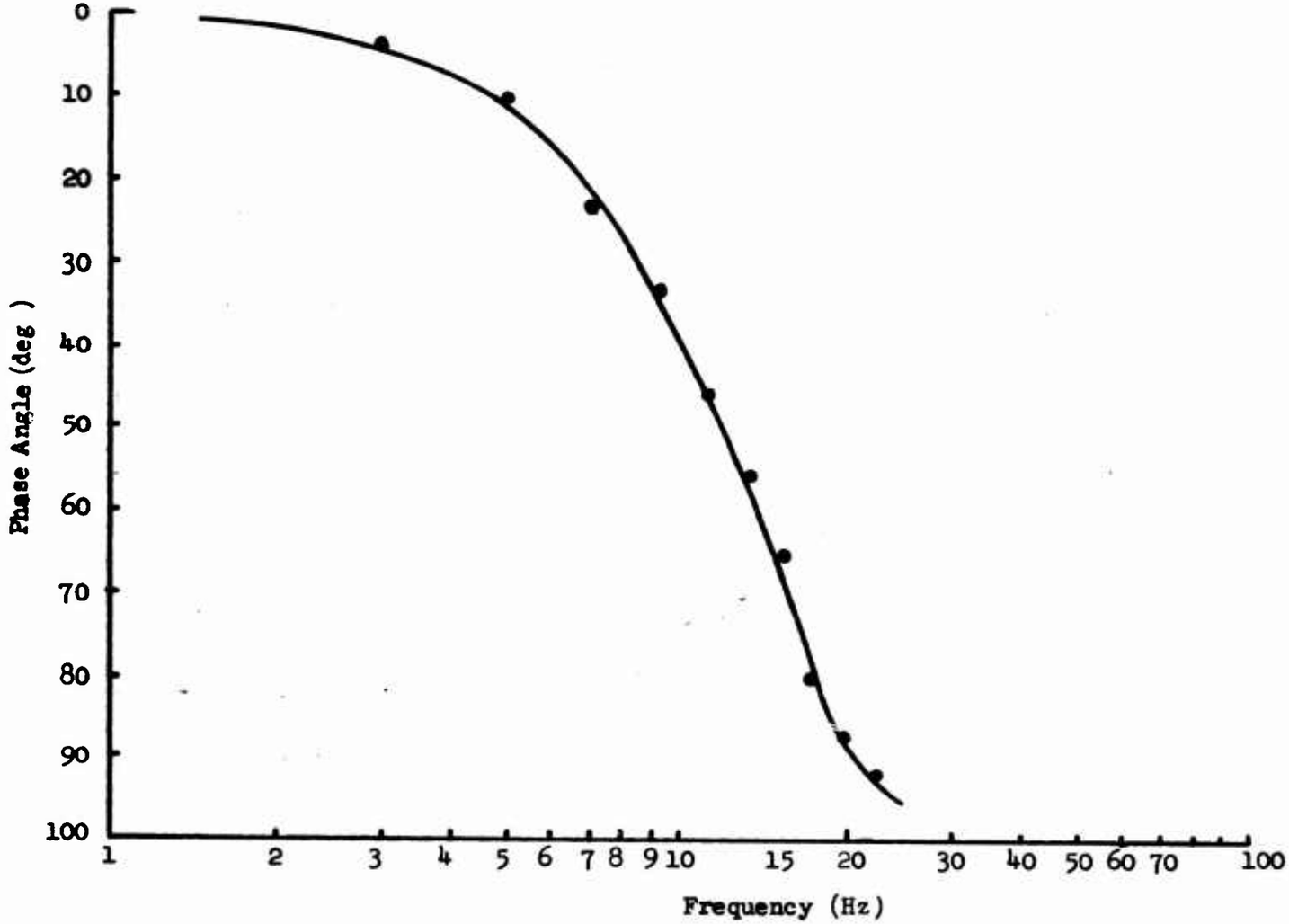

Figure 44. Integral Armored Servo Phase Angle Lag.

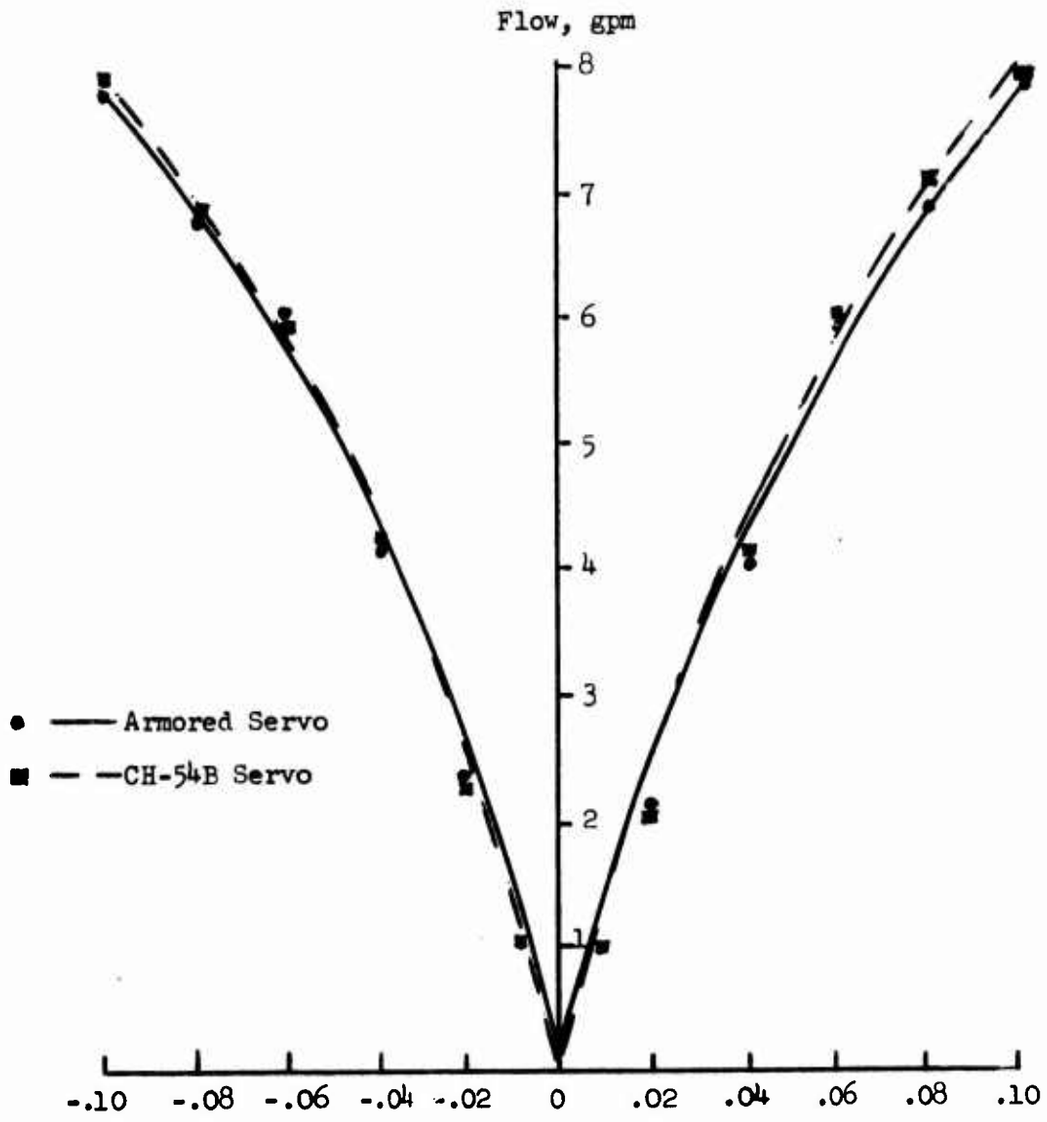

Figure 45. Servo Valve Flow Gain.

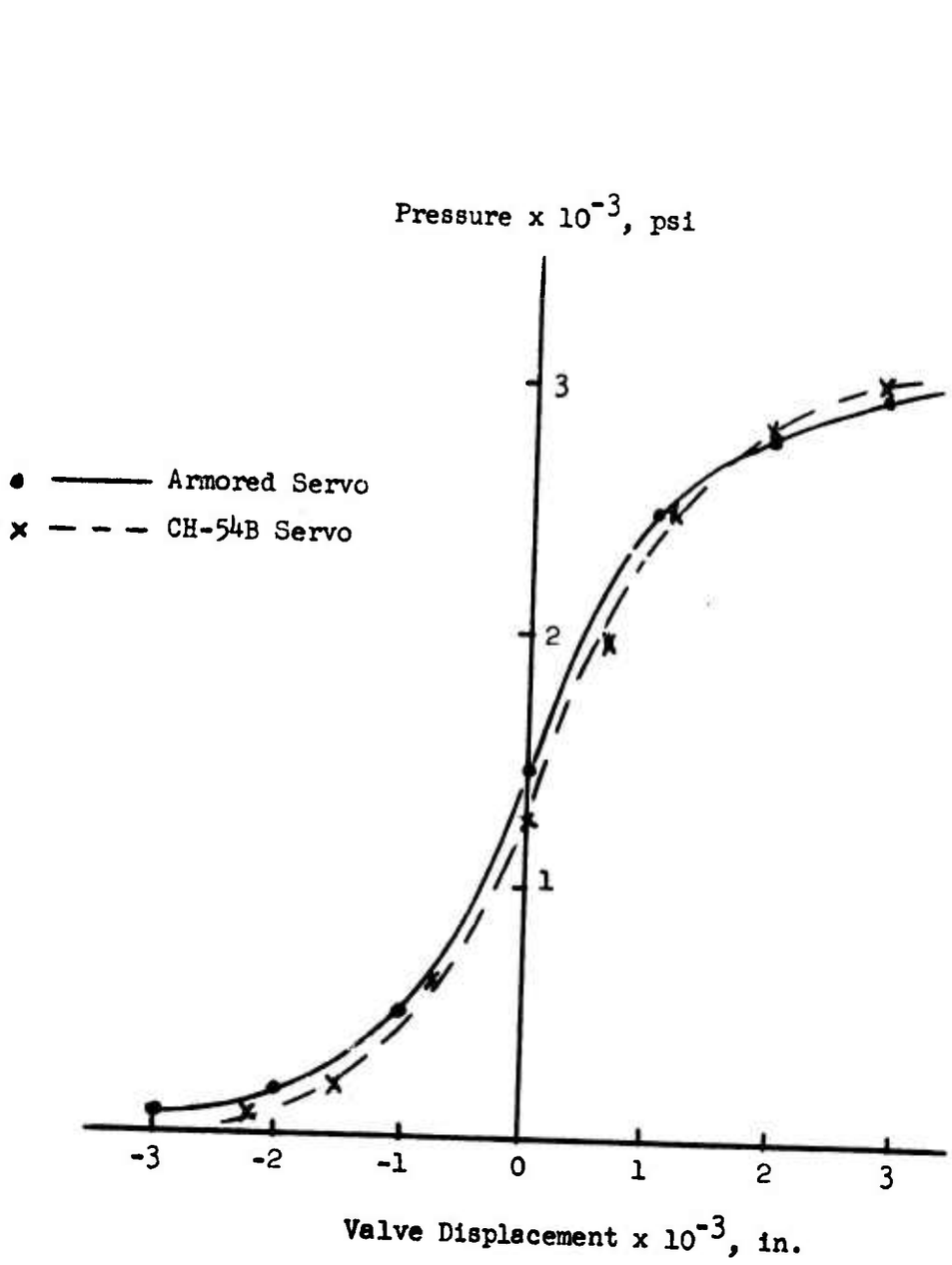

Figure 46. Servo Valve Pressure Gain.

TEST LOG

INTEGRAL ARMORED SERVO

Test		Date Completed	Technician
2.0(1)	Valve, Pressure Gain	7/13/71	W. Larkin
2.0(2)	Valve, Flow Gain	7/13/71	W. Larkin
2.0(3)	Valve, Spool Forces	10/28/71	P. Targonski
3.0(1)	Servo, Proof Press	11/11/71	P. Targonski
3.0(2)	Servo, Int. Leakage	10/18/71	P. Targonski
3.0(3)	Servo, Ext. Leakage	10/18/71	P. Targonski
3.0(4)	Servo, Input Force	10/18/71	P. Targonski
3.0(5)	Servo, Linkage Spring Rate	10/18/71	P. Targonski
3.0(6)	Servo, Response Char.	10/15/71	P. Targonski
3.0(7)	Servo, Actuator Stroke	10/18/71	P. Targonski

Actuator Stroke

Maximum Extend Position 0.0

Maximum Retract 5.375 in.

Armored Servo - Servo Valve Spool Force Test

P/N 38650-11019-041 S/N 4

Equipment: Servo Valve Test Fixture
0-1602 Spring Scale (S/N50)

Results: Press., 3,000 psi

Fluid Temp, 90°F to 110°F

Push from C_1 to C_2 2.5 ounces

Push from C_2 to C_1 2.0 ounces

Input Linkage Spring Rate

Block Servo Housing

Apply a force to the input link and measure deflection

Set dial indicator to zero at 200 lb to eliminate slop.

F	300	400	500	200	Side deflection of mounting .0065 in.
X	.0044	.014	.023	.000	
	1	2	3	4	

X = 15,000 lb /in.

Input Force

Ambient temperature 70°F; fluid temperature 80°F.

	1st Stage	2nd Stage	1st and 2nd Stages
f_{in} (lb)	4.0	3.5	3.25
f_{out} (lb)	2.25	2.2	3.5

Internal Leakage

Fluid Temp, 100°F

Piston Centers	960 cc/min	1,570 cc/min
Piston Against Stop	400 cc/min	1,120 cc/min
	First Stage	Second Stage

External Leakage

Fluid Pressure, 3,000 psi

Fluid Temp, 80°F

	Drops Per 25 Cycles
Upper End Cap	1
Lower End Cap	2
Separator Vent	3
Input Shaft Vent	0
Transfer Tubes	1/2
Others	

Proof Pressure

Abnormalities

None

Pressure (fluid), 4,500 psi

Temp. (fluid), 110°F

INSTRUMENTATION RECORD

Frequency Response Test Instrumentation

Hydraulic Test Stand Sikorsky Design
3,000 psi, 30 gpm max

Servomatic Analyzer Model 1995
Servo Corporation of America
S.A. Calibration #M02735

Oscilloscope
Hewlett-Packard Model 130B
S.A. Cal. #M03760

Osc.
H.P. Model 130B
S.A. #M02896

DC Microvolt-Ammeter
Dynamics Instrument Corporation
Model 4072
S.A. #M02276

DISTRIBUTION

Director of Defense Research & Engineering	2
Assistant Secretary of the Army (R&D)	1
Assistant Chief of Staff for Force Development, DA	2
Deputy Chief of Staff for Logistics, DA	1
Chief of Research & Development, DA	2
Army Materiel Command	5
Army Aviation Systems Command	13
Hq, Army Air Mobility R&D Laboratory	2
Ames Directorate, Army Air Mobility R&D Laboratory	2
Eustis Directorate, Army Air Mobility R&D Laboratory	15
Langley Directorate, Army Air Mobility R&D Laboratory	2
Lewis Directorate, Army Air Mobility R&D Laboratory	2
Army Aviation Systems Test Activity	2
Army R&D Group (Europe)	2
Army Scientific & Technical Information Team (Europe)	1
Army Advanced Materiel Concepts Agency	1
Harry Diamond Laboratories	1
Army Ballistic Research Laboratory	3
Army Research Office - Durham	1
Army Materials & Mechanics Research Center	8
Army Test & Evaluation Command	1
USACDC Aviation Agency	3
USACDC Transportation Agency	1
Army Tank-Automotive Command	2
Army Weapons Command	1
Army Command & General Staff College	1
Army Aviation School	1
Army Agency for Aviation Safety	1
Army Field Office, AFSC	1
Air Force Office of Scientific Research	1
Air Force Armament Development & Test Center	1
Air Force Materials Laboratory	3
Air Force Flight Dynamics Laboratory	7
Aeronautical Systems Division, AFSC	2
Air Force Institute of Technology	1
Naval Air Systems Command	12
Chief of Naval Research	3
Naval Research Laboratory	2
Naval Air Development Center	3
Naval Weapons Center	1
Naval Weapons Laboratory	1
Naval Ship Research & Development Center	2
Commandant of the Marine Corps	1
Marine Corps Development & Education Command	1
Marine Corps Liaison Officer, Army Transportation School	1
Defense Documentation Center	2

UNCLASSIFIED

Security Classification

DOCUMENT CONTROL DATA - R & D

(Security classification of title, body of abstract and indexing annotation must be entered when the overall report is classified)

1. ORIGINATING ACTIVITY *(Corporate author)*
Sikorsky Aircraft Division
United Aircraft Corporation
Stratford, Connecticut

2a. REPORT SECURITY CLASSIFICATION
Unclassified

2b. GROUP

3. REPORT TITLE
DESIGN, FABRICATION, AND PERFORMANCE TESTING OF INTEGRAL ARMORED SERVO ACTUATORS

4. DESCRIPTIVE NOTES *(Type of report and inclusive dates)*
Final Report

5. AUTHOR(S) *(First name, middle initial, last name)*
Karl Wallischeck
George R. Karas

6. REPORT DATE	7a. TOTAL NO. OF PAGES	7b. NO. OF REFS
April 1972	114	-

8a. CONTRACT OR GRANT NO.	9a. ORIGINATOR'S REPORT NUMBER(S)
DAAJ02-70-C-0051 New	
b. PROJECT NO. 1F164204D154	USAAMRDL Technical Report 72-15
c.	9b. OTHER REPORT NO(S) *(Any other numbers that may be assigned this report)*
d.	SER-50759

10. DISTRIBUTION STATEMENT
Distribution limited to U. S. Government agencies only; test and evaluation; April 1972. Other requests for this document must be referred to the Eustis Directorate, U. S. Army Air Mobility Research and Development Laboratory, Fort Eustis, Va. 23604.

11. SUPPLEMENTARY NOTES	12. SPONSORING MILITARY ACTIVITY
	Eustis Directorate, U. S. Army Air Mobility Research and Development Laboratory, Fort Eustis, Virginia

13. ABSTRACT

A program was conducted to demonstrate and establish the applicability of using dual property steel armor (DPSA) integrally in complex Army aircraft critical components, thus eliminating or minimizing the requirement for adding armor plate (shielding) to protect these components from small-arms ballistic impacts. A CH-54B primary flight control hydraulic servo actuator was selected as the critical component and was redesigned using DPSA as the cylinder material. Three experimental units were fabricated and tested.

DD FORM 1 NOV 68 1473 REPLACES DD FORM 1473, 1 JAN 64, WHICH IS OBSOLETE FOR ARMY USE.

UNCLASSIFIED

Security Classification

14. KEY WORDS	LINK A		LINK B		LINK C	
	ROLE	WT	ROLE	WT	ROLE	WT
Servo actuator						
Dual property steel armor						
Aircraft components						
Ballistic tolerance						
Flight controls						
Small-arms ballistic impacts						
CH-54B						
DPSA						